1961

The mass spectra of some volatile hydrides

Fred Eric Saalfeld
Iowa State University

THE MASS SPECTRA OF SOME VOLATILE HYDRIDES

by

Fred Eric Saalfeld

A Dissertation Submitted to the
Graduate Faculty in Partial Fulfillment of
The Requirements for the Degree of
DOCTOR OF PHILOSOPHY

Major Subject: Physical Chemistry

Approved:

Signature was redacted for privacy.

In Charge of Major Work

Signature was redacted for privacy.

Head of Major Department

Signature was redacted for privacy.

Dean of Graduate College

Iowa State University
Of Science and Technology
Ames, Iowa

1961

TABLE OF CONTENTS

		Page
I.	DESCRIPTION OF THE MASS SPECTROMETER	1
	A. Introduction	1
	B. The Ion Source	1
	C. Mass Analyzer Tube	3
	D. Collector	4
	E. The Electromagnet	5
	F. Mass Spectrometer's Vacuum System	7
	G. Gas Sample System	7
	H. Electrical Circuits	8
	1. High voltage supply	8
	2. Emission regulator	9
	3. Preamplifier, amplifier and recorder	9
	4. Magnet power supply	20
	5. Cold cathode gauge control	20
II.	SILANE	31
	A. Introduction	31
	B. Experimental	33
	1. Preparation	33
	2. Mass spectral properties	34
	a. Fragmentation pattern	34
	b. Appearance potentials	38
	c. Cross-sections	45
III.	GERMANE	50
	A. Introduction	50
	B. Experimental	52
	1. Preparation	52
	2. Mass spectral properties	54
	a. Fragmentation pattern	54
	b. Appearance potentials	71
	c. Cross-sections	76
IV.	STANNANE	78

		Page
V.	PLUMBANE	82
	A. Introduction	82
	B. Experimental	82
VI.	PHOSPHINE	84
	A. Introduction	84
	B. Experimental	86
	1. Preparation	86
	2. Mass spectral properties	87
	a. Fragmentation patterns	87
	b. Appearance potentials	93
	c. Cross-sections	97
VII.	ARSINE	99
	A. Introduction	99
	B. Experimental	101
	1. Preparation	101
	2. Mass spectral properties	101
	a. Fragmentation patterns	101
	b. Appearance potentials	107
	c. Cross-sections	111
VIII.	STIBINE	112
	A. Introduction	112
	B. Experimental	114
	1. Preparation	114
	2. Mass spectral properties	116
	a. Fragmentation pattern	116
	b. Appearance potentials	121
	c. Cross-sections	125
IX.	BISMUTHINE	126
	A. Introduction	126
	B. Experimental	126
X.	SUMMARY	128

Page

XI. BIBLIOGRAPHY 129

XII. ACKNOWLEDGEMENTS 134

XIII. APPENDICES 135

A. Appendix A: Comparison of the Fragmentation Patterns and Bond Energies of the Group IVB Hydrides 135

B. Appendix B: Heats of Formation and Average M-H Bond Energies of the Group IVB Hydrides 138

C. Appendix C: Comparison of the Fragmentation Patterns and Bond Energies of the Group VB Hydrides 139

D. Appendix D: Heats of Formation and Average M-H Bond Energies of the Group VB Hydrides 142

I. DESCRIPTION OF THE MASS SPECTROMETER

A. Introduction

While the description of the mass spectrometer used in this study is certainly relevant, the thesis is not primarily concerned with the theory and construction of the instrument, so the discussion of this topic will be as brief as possible. Many of the major components were obtained commercially and will be described by reference to their manufacturer's technical bulletins. The reader should bear in mind that the present instrument is very similar to the mass spectrometer described by Svec (1) and, for further information pertaining to the theory and construction aspect of this problem, attention is called to this reference as well as the many excellent reference books now available (2,3,4).

B. The Ion Source

The ion source used in this mass spectrometer is similar to that discussed by Svec (1). Ionizing electrons are emitted from a heated tungsten ribbon, pass through the ionization chamber, and are collected by the trap electrode. The current created by the flow of these electrons can be measured between the filament and shield as total emission, and between the filament and trap as ionizing current.

A magnetic field of approximately 125 gauss arising from two Alnico V poles mounted on an iron yoke just outside the ion source envelope, serves to collimate the electron beam. The trap electrode is made of Armco iron to concentrate the magnetic field and thus facilitate the collection of electrons.

The principal difference between this ion source and the one discussed by Svec is the inclusion of a repeller electrode. This device enables the operator to have an additional degree of control over the ion beam. The initial energies of fragment ions can be estimated by observing a fragment ion current as a function of the potential applied to this electrode according to the method described by Taubert (5). Since a knowledge of the presence or absence of initial kinetic energy of fragment ions is extremely important for determining bond energies and heats of formation from appearance potential data, the inclusion of the repeller electrode was desirable. The surfaces of the ion source involved in accelerating electrons is painted with Aquadag (Acheson Colloids Corp., Port Huron, Michigan), an aqueous colloidal graphite suspension. Aquadag gives a good uniform conducting surface throughout the entire ionization chamber and overcomes deleterious effects due to the formation of insulating materials such as tungstic oxide. This greatly improves the emission characteristics of the source.

The arrangement of the ion accelerating and focusing

slits is similar to that discussed by Svec (1). In the present instrument the source envelope is made of non-magnetic stainless steel (Type 302) designed in such a manner that removal of the cover of the envelope will expose the entire source assembly. The advantages of this arrangement are obvious. The trunk of the envelope was soldered to a copper analyzer tube using high melting (m.p.$\approx$1300°F) silver solder. The cover and trunk are closed by means of an aluminum gasket fitted in appropriate flanges. The electrical leads to the ion source enter the envelope through two seven-lead bulkheads (Fusite Series 9-700, The Fusite Corporation, Cincinnati, Ohio). A vacuum tight seal is obtained between the bulkheads and envelope by means of aluminum gaskets. The entire assembly design is similar to a standard tubing flare-fitting using a modified nut to apply pressure between the bulkhead and gasket. The assembly is bakeable and demountable.

C. Mass Analyzer Tube

The mass analyzer tube is a one inch copper tube, 71.8 centimeters long, bent in the center through an angle 120° in a 15 centimeter radius. Four-and-one-half inches of each end of the tube are perforated with many one-eighth inch diameter holes to facilitate the evacuation of the tube. The center portion of the tube is flattened to approximately

a half an inch.

D. Collector

Due to difficulty observed by Svec (1) with the collector plate system originally designed by Nier, a Faraday cup type of collector was employed in the present instrument. The collector assembly is supported by two line-up studs and two 2-56 screws which are mounted on the base plate of the collector. These studs and screws attach the collector assembly to the analyzer tube. The spacing between the plates in the collector is maintained by accurately ground pyrex glass spacers.

The collector slit is constructed so that the slit width may be varied accurately. The original single collector, similar in design to the collector in the General Electric analytical mass spectrometer, was modified in these laboratories so that the adjustment of the collector slit could be achieved and measured with a micrometer. The modification consisted of replacing the original screw adjustment with a spring loaded drive mechanism. The screw mechanism originally on the slit was discarded, leaving the top half of the slit free to slide in the original grooves. A bellows, mounted in the stainless steel collector envelope, was attached to a small rod which was also connected to the moveable side of the slit. Then, with the slit open to its

maximum width, the rod from the bellows was connected in such a manner that the slit remained at this width. On the outside of the envelope the micrometer was mounted so that when it was attached to the envelope, the bottom of the micrometer just rested on an anvil attached to the top of the bellows. As the micrometer is turned down, the bellows is compressed, pushing the slit closed. When the micrometer is returned to its original position, the bellows expands and the slit is opened. The size of the slit is read directly from the micrometer calibrations.

The electrical leads from the collector pass through the envelope by means of two single-lead high voltage terminals (CC-907-SS-HV-Electrical Industries, Murray Hill, New Jersey) silver soldered to the envelope with high melting solder. One lead is connected to the preamplifier through a coaxial tube and the second lead to the secondary electron suppressor electrode which is maintained at a potential of 45 volts below ground under normal operating conditions.

E. The Electromagnet

The mass analyzer tube of the instrument was mounted in such a manner that a straight line drawn between the exit slit of the ion source and the collector slit would pass through the apex of the magnetic field and would be

horizontal. To accomplish this the electromagnet was placed in a vertical position. Since the mass tube was to be adjusted by moving the tube itself, the magnet was permanently positioned. This was done by mounting the magnet on a steel base which can be leveled by means of screws. The yoke of the magnet and the cylindrical poles were bolted to the base plate.

Mild steel, SAE 1020, was used to construct the yoke and the cylindrical poles (1) while the pole pieces were made from hot rolled Armco magnetic iron (Corey Steel Co., Chicago 80, Illinois). None of the dimensions are critical but the faces of the pole pieces must be parallel to each other to keep the magnetic field as uniform as possible. The choice of the 3-15/16 inch cylindrical poles was made so that some of the equipment on hand in these laboratories could be used (1). Each of the coils of the electromagnet was wound with 20,000 turns of Heavy Formvar insulated copper wire (A.W.G. 22, Anaconda Wire and Cable Company, Chicago, Illinois). Connected in series, these coils have a resistance of approximately 1000 ohms at room temperature. A current of 500 milliamperes passing through these coils produces a field of 5100 gauss. This current is supplied to the coils from an electronic, variable current magnet power supply which is mounted in the main cabinet.

F. Mass Spectrometer's Vacuum System

The mass tube of the instrument is evacuated by means of an all metal, high speed, mercury diffusion pump (MHG-40, Consolidated Electrodynamics Corporation, Rochester, New York). A cold cathode ion gauge (Miller Laboratories, Latham, New York) is used to monitor the pressure in the mass tube. The controls of the ion gauge are mounted in the main cabinet.

The MHG-40 pump is backed by a mechanical fore pump. There is a glass trap, cooled with liquid nitrogen, between the diffusion pump and the mass tube and a ballast between the diffusion pump and the fore pump. No arrangements have been made for baking the analyzer tube since with the present arrangement a pressure of 2×10^{-8} torr can be obtained when the system is clean.

G. Gas Sample System

The inlet system of the instrument consisted of two viscous leaks, each made of a five-inch length of copper capillary tubing, 0.005 inch internal diameter. The leaks are terminated by adjustable constrictions. These leaks enable the operator to allow two different samples to flow into the instrument simultaneously. The gas in the sample system can be pumped independent of the mass tube by means of an air cooled oil diffusion pump backed by a

mechanical fore pump. Both of these pump the sample system through a ballast. Each side of the above mentioned valves can be pumped independent of each other since four Hoke valves (No. 413 AXD 9218 Hoke, Inc., Cresskill, New Jersey) are placed between the ballast and the sample valves. The pressure in the sample system is monitored by means of a thermocouple vacuum gauge (model G V 3RS, Hastings-Raydist, Inc., Hampton, Virginia). The controls for this gauge are mounted in the main cabinet.

The sample flows from the sample system to the mass spectrometer through twenty-four inches of one-fourth inch copper tubing. The size of the orifice is reduced to one-eighth inch in diameter through the source envelope. This latter tube leads to the top of the ionization chamber and is electrically insulated from the shield by means of a close fitting glass tube.

H. Electrical Circuits

1. High voltage supply

With the exception of a few minor changes to be mentioned below, the high voltage supply and voltage divider are identical to those described by Svec (1).

A string of three resistors, in series, have been added to the supply across the capacitors C_2 and C_3. (In the following, all components will be referred to using Svec's

notation (1)). The center resistor is a 100K, 10 turn helical potentiometer and the others are 250K precision resistors. The wiper of the helical potentiometer is connected to the grid of V_4. This change enables the operator to adjust the voltage to the shield independently of the voltage divider. The switch S_5 and the capacitor C_9 have been replaced by another 100 K helical potentiometer by means of which varying potentials can be applied to the repeller electrode. The present circuit is shown in Figure 1.

2. Emission regulator

The theory and use of the emission regulator has been fully discussed by Svec (1). While the emission regulator in the present instrument follows these principles basically, the circuitry has been sufficiently changed to justify a circuit diagram which is shown in Figure 2.

3. Preamplifier, amplifier and recorder

The preamplifier and first amplifier used in the instrument is a vibrating reed electrometer (model 36, Applied Physics Corporation, Pasedena, California) and is fully described in their bulletin. This electrometer has an input resistor whose nominal value is 10^{12} ohms. The circuit is shown in Figure 3 and the schematic arrangement in Figures 4 and 5. The ion current is further amplified

Figure 1. High voltage supply and voltage divider

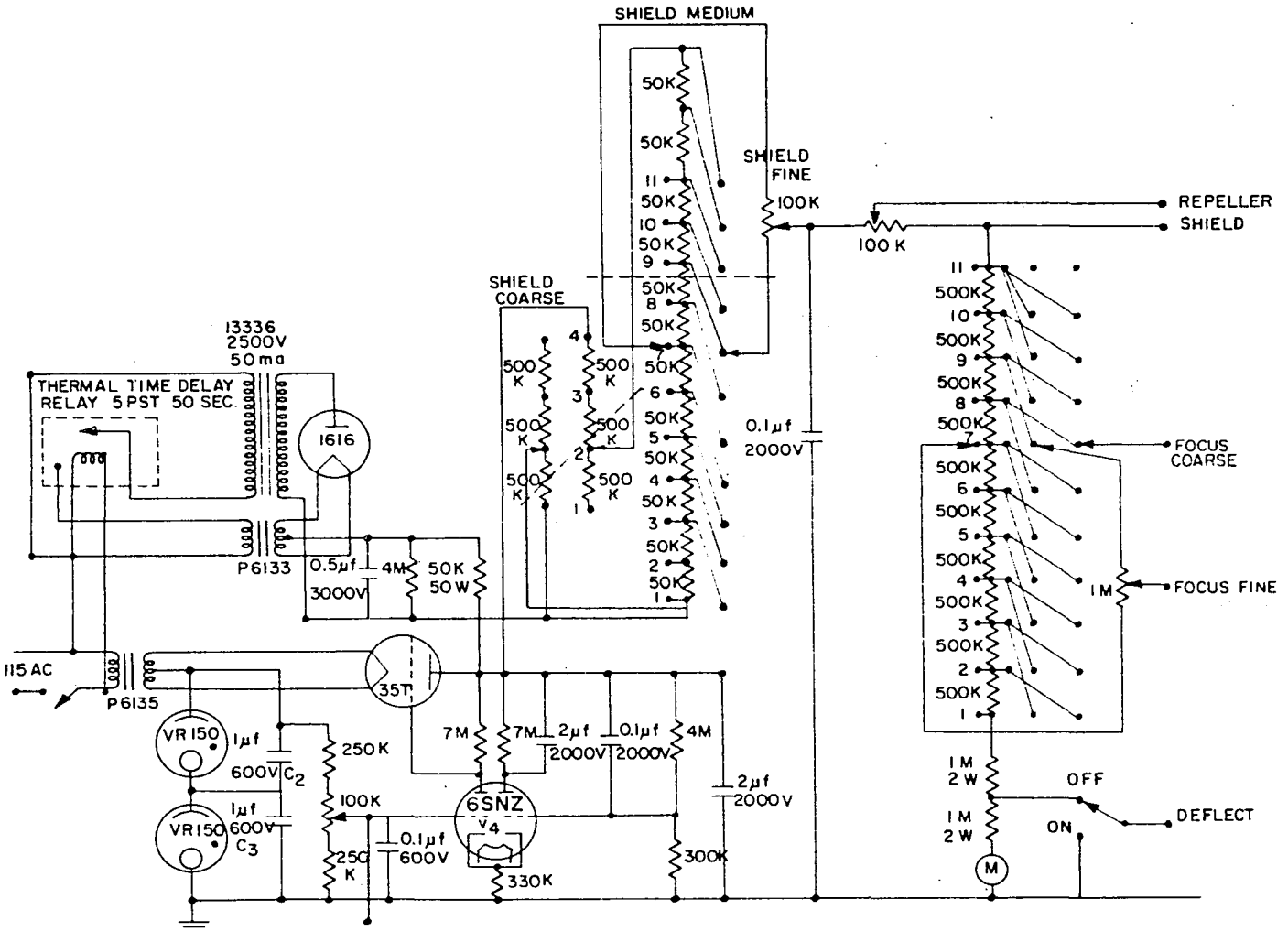
SHIELD MEDIUM
SHIELD FINE
SHIELD COARSE
50K
100K
REPELLER
SHIELD
100 K
0.1μf
2000V
FOCUS COARSE
FOCUS FINE
1M
500K
13336
2500V
50 ma
THERMAL TIME DELAY
RELAY 5PST 50 SEC.
1616
P6133
0.5μf
3000V
4M
50K
50 W
115 AC
P6135
35T
VR150
1μf
600V
C2
C3
250K
100K
250K
0.1μf
600V
6SNZ
V4
330K
7M
2μf
2000V
0.1μf
2000V
4M
2μf
2000V
300K
1M
2W
OFF
ON
DEFLECT
M

Figure 2. Emission regulator

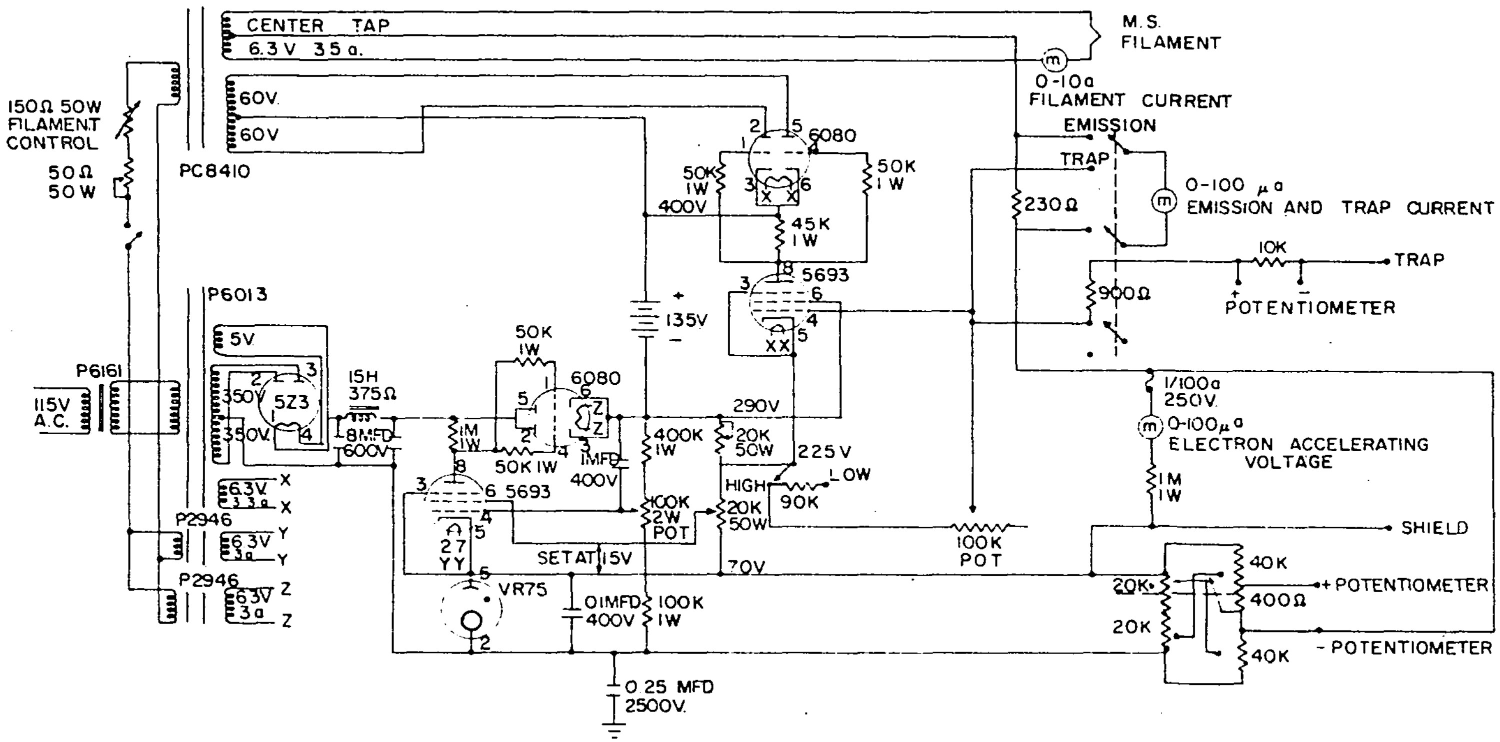
CENTER TAP
6.3V 35a.
M.S.
FILAMENT
0-10a
FILAMENT CURRENT
60V
60V
150Ω 50W
FILAMENT
CONTROL
50Ω
50W
PC8410
EMISSION
TRAP
6080
50K
1W
50K
1W
400V
45K
1W
230Ω
0-100 μa
EMISSION AND TRAP CURRENT
10K
TRAP
5693
900Ω
POTENTIOMETER
P6013
5V
135V
P6161
115V
A.C.
350V
350V
5Z3
15H
375Ω
8MFD
600V
50K
1W
6080
50K 1W
1M
1W
1MFD
400V
290V
400K
1W
20K
50W
225V
LOW
HIGH
90K
100K
2W
POT
20K
50W
5693
27
YY
SET AT 15V
70V
100K
POT
1/100a
250V.
0-100μa
ELECTRON ACCELERATING
VOLTAGE
1M
1W
SHIELD
40K
+ POTENTIOMETER
400Ω
20K
20K
40K
- POTENTIOMETER
6.3V
3.3a
X
X
P2946
6.3V
3a
Y
Y
P2946
6.3V
3a
Z
Z
VR75
.01MFD
400V
100K
1W
0.25 MFD
2500V.

Figure 3. Electrical circuit of the vibrating reed model 36 electrometer

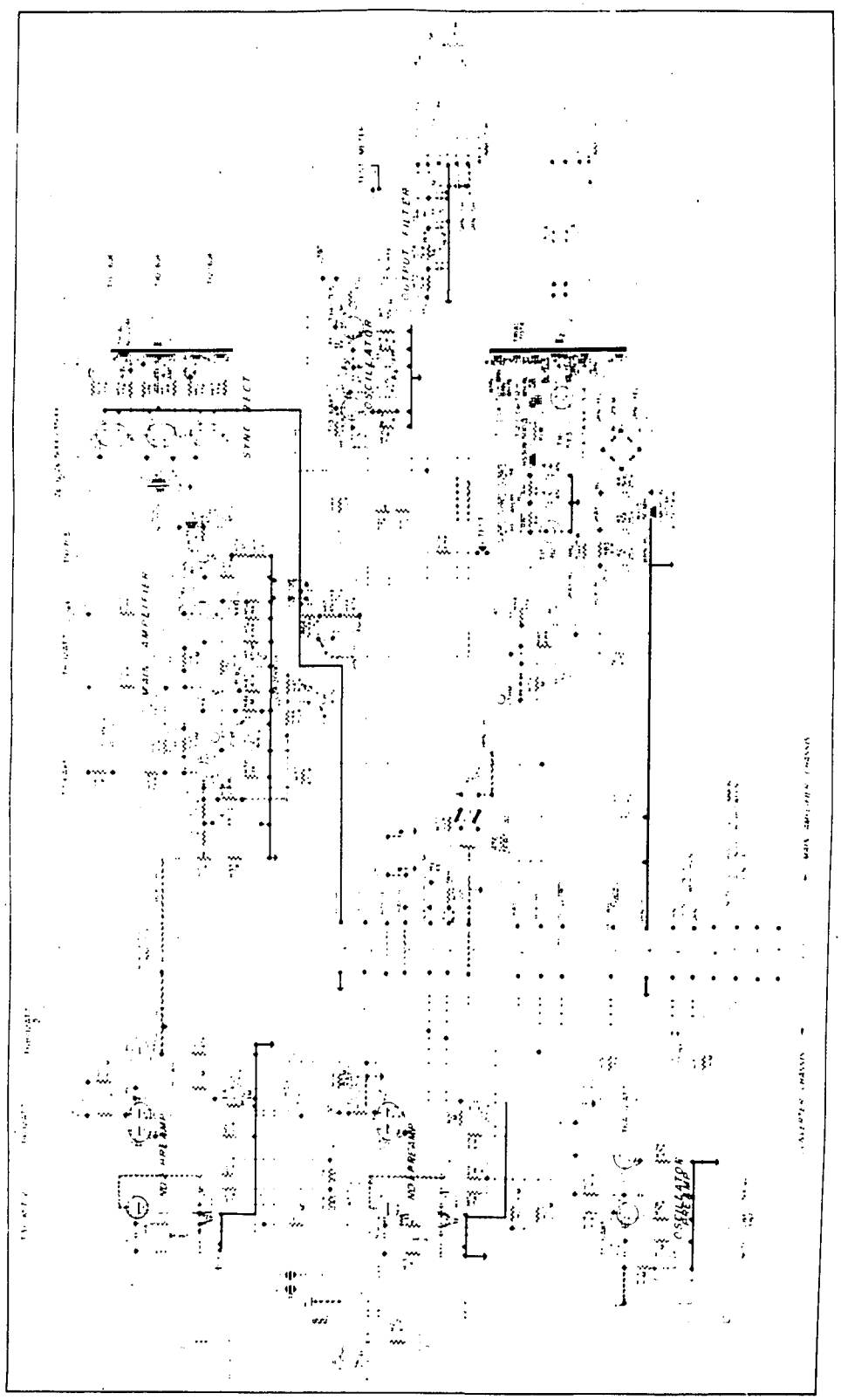

Figure 4. Component boards of model 36 electrometer

R 33	2200	R 71	550 Ω
R 34	47 K	R 73	50 K
R 35	270 K	R 74	50 K
R 36	270	R 75	220 Ω
R 37	470 K	R 77	22 K
R 38	1 K	R 78	68 K
R 39	56 K	R 79	1.0 M
R 41	10 K	R 80	6 K
R 42	47 K	R 81	4 K
R 43	3.9 M	R 82	5 Ω
R 44	8.2 K	R 83	10 K
R 45	8.2 K	R 84	33 K
R 46	1.0 M	R 85	68 K
R 47	47 K	R 86	10 K
R 48	100 K	R 87	2200
R 49	10 M	R 88	22 K
R 50	82 K		
R 51	470 K		
R 52	6.8 K		
R 53	68 K		
R 54	1.8 K		
R 55	2 70 K	C 22	0.002
R 56	450 Ω	C 13	0.01
R 57	100 Ω	C 14	0.0001
R 58	33 K	C 16	(A2) 0.10
R 59	33	C 18	0.0001
R 60	18 K	C 19	0.01
R 61	18 K	C 21	0.002
R 62	33 K	C 24	0.002
R 63	33 K	C 25	0.047
R 66	4.7 K	C 30	0.001
R 67	100 K	C 31	(A2) 0.01
R 68	270 K	C 32	0.05
R 69	1 K	C 33	(A2) 0.005
R 70	270 K	C 39	0.01
* R 40	47	C 45	0.01
* R 72	47	C 46	0.05
		C 47	0.05
		C 48	0.02
		C 49	0.001
		C 50	0.005
		C 37	100
		C 52	20 pfd

* MOUNTED ON TUBE SOCKET

Figure 5. Rear view of model 36 electrometer

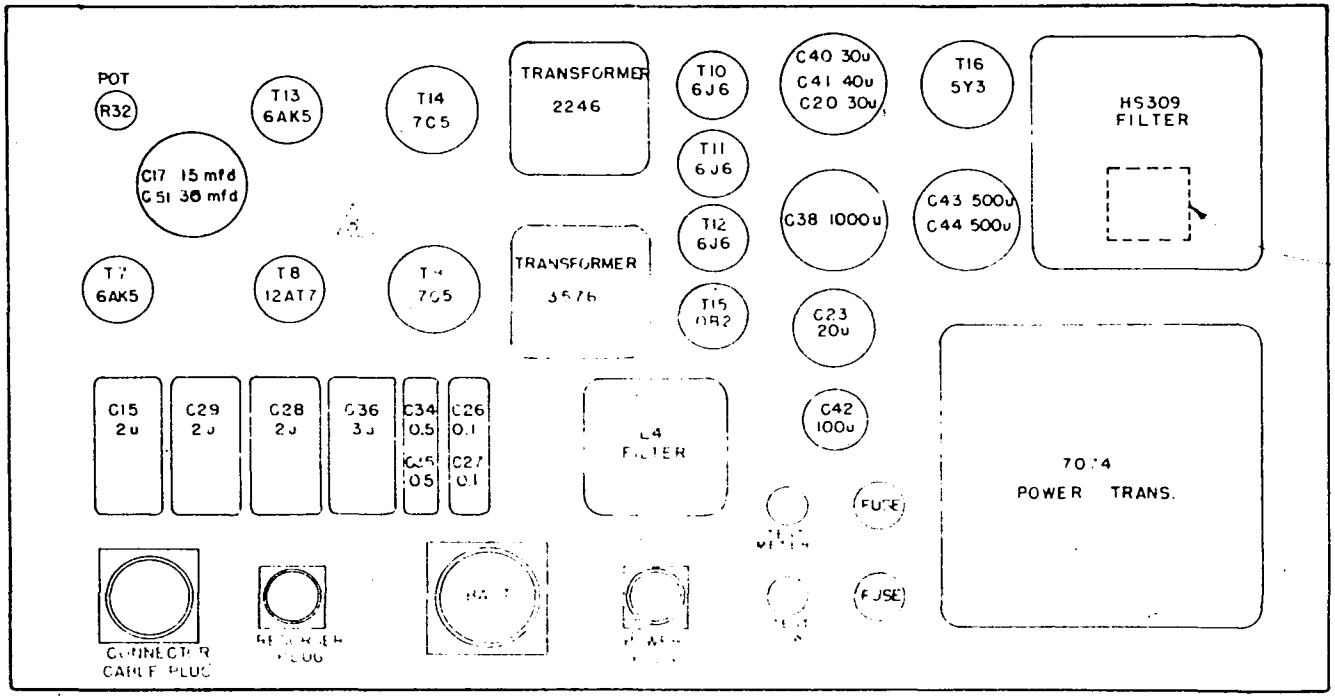
POT
R32
T13
6AK5
T14
7C5
TRANSFORMER
2246
T10
6J6
T11
6J6
T12
6J6
T15
0B2
C40 30u
C41 40u
C20 30u
T16
5Y3
HS309
FILTER
C17 15 mfd
C 51 36 mfd
C38 1000u
C43 500u
C44 500u
T7
6AK5
T8
12AT7
T9
7C5
TRANSFORMER
3576
C23
20u
C15
2u
C29
2u
C28
2u
C36
3u
C34
0.5
C35
.05
C26
0.1
C27
0.1
C42
100u
L4
FILTER
7074
POWER TRANS.
FUSE
FUSE
CONNECTOR
CABLE PLUG
(FAR SIDE)
HT48 OR TE7904
FILTER

REAR VIEW

by means of an impedance matching amplifier (KinTel, a division of Cohu Electronics, Inc., San Diego, California, model 111BF). While it is adequately described in Kin Tel's technical manual code number 2x-51, its circuit is shown here in Figure 6 for convenience.

A Weston recorder, model 6701, modified to have a continuous drive chart is used to record the mass spectrum. The recorder has been converted from a 10 millivolt recorder to a 100 millivolt one to reduce the noise to signal level. The arrangement of these three components is shown schematically in Figure 7. The voltage divider which enables the operator to attenuate the recorder is also shown.

4. Magnet power supply

The magnet power supply was built in the electronic shop of these laboratories. This supply enables the current through the magnet coils to be varied from zero to 500 milliamperes. The circuits for this supply are shown in Figures 8 and 9.

5. Cold cathode gauge control

The cold cathode vacuum gauge is a commercial unit supplied by the Miller Laboratories of Latham, New York, model number 100. While the description of this control is discussed adequately in the bulletin supplied by the company, it is not easily obtainable therefore a circuit diagram is shown in Figure 10.

Figure 6. Schematic diagram of model 11BF amplifier

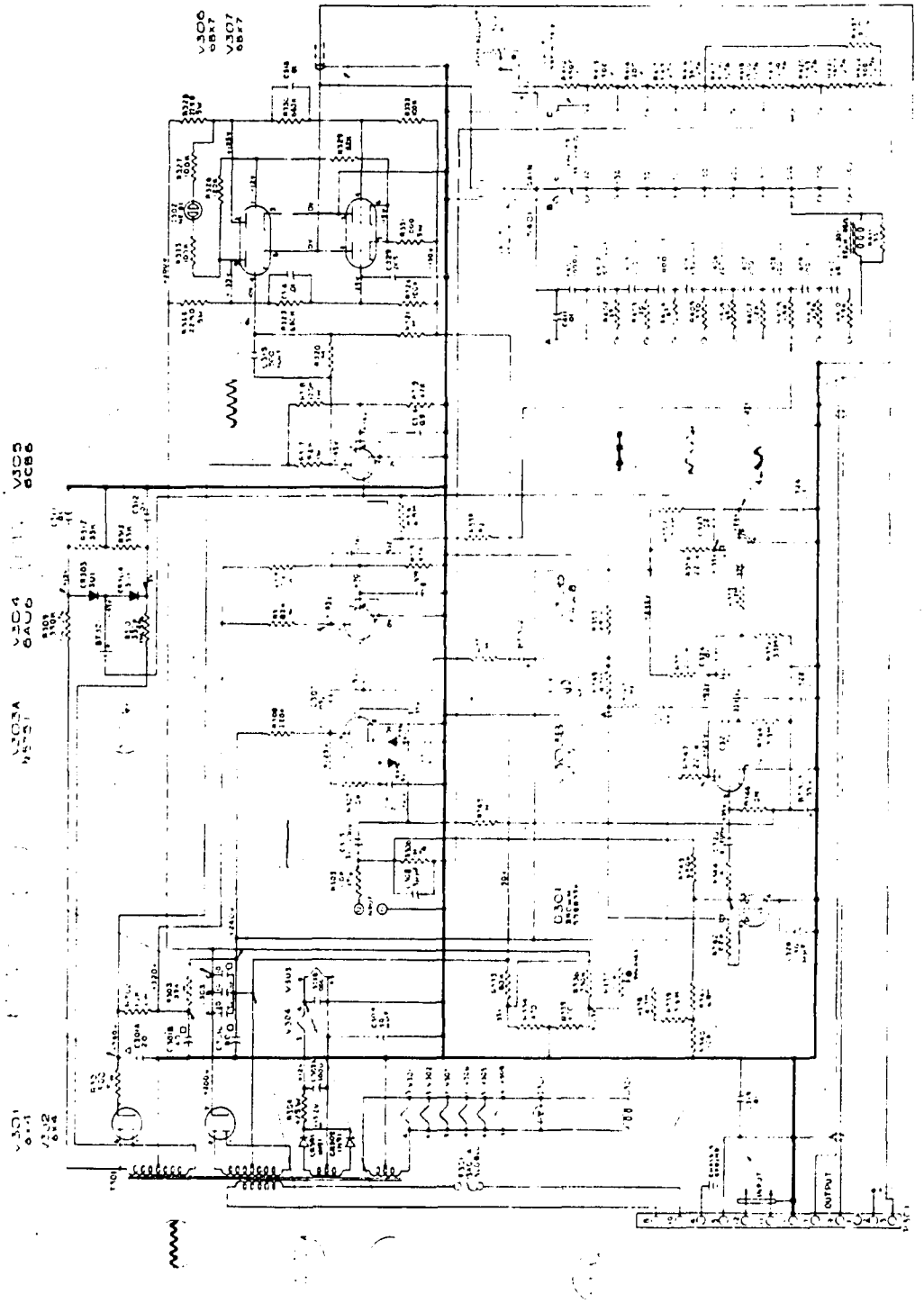
V306
6BX7
V307
6BX7
V305
6CB6
V304
6AU6
V303A
V303B
V301
V302
OUTPUT

Figure 7. Schematic diagram of attenuation circuit

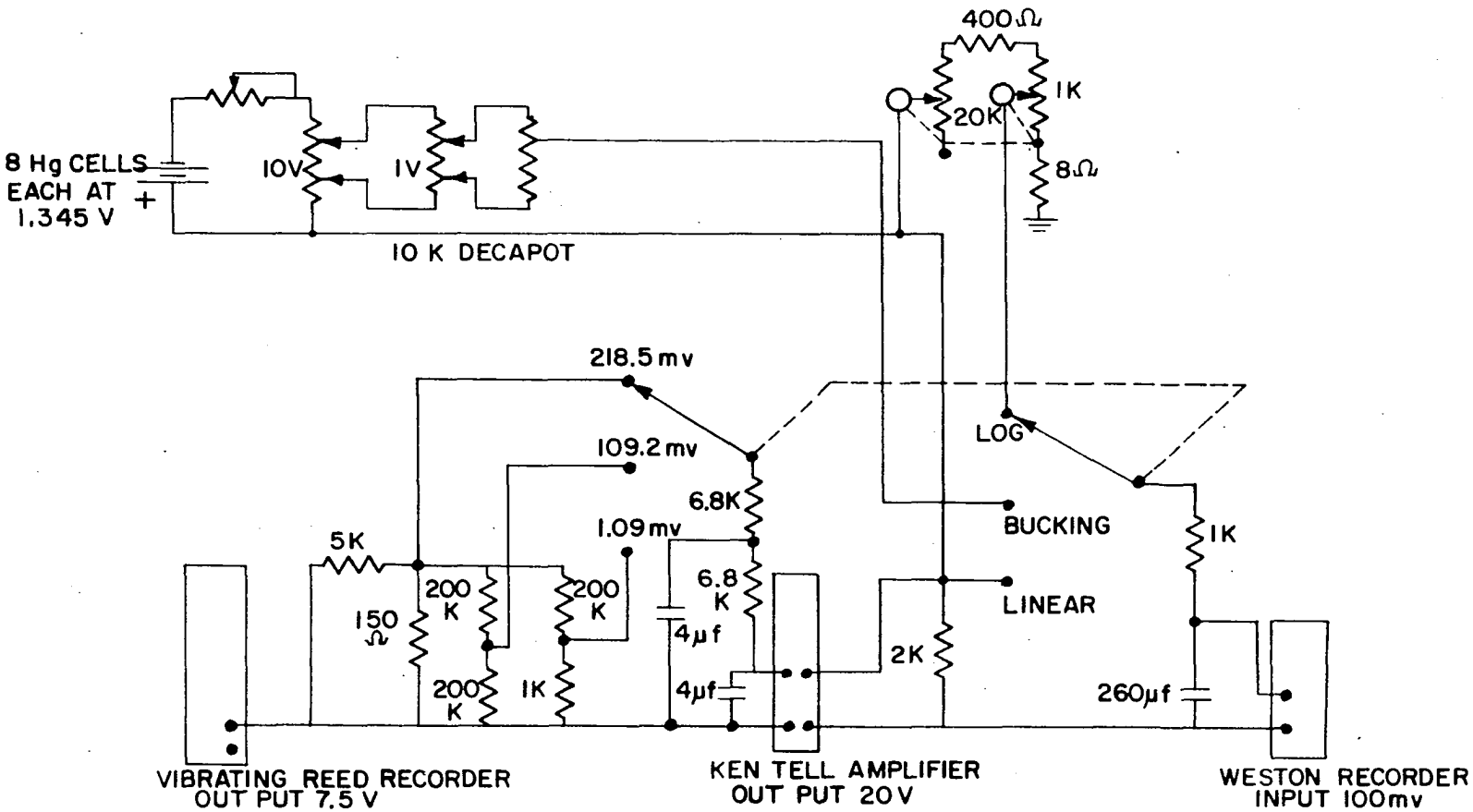
400Ω
1K
20K
8Ω
8 Hg CELLS
EACH AT
1.345 V
+
10V
1V
10 K DECAPOT
218.5 mv
109.2 mv
1.09 mv
LOG
6.8K
BUCKING
5K
200
K
200
K
150
Ω
200
K
1K
6.8
K
4μf
4μf
2K
LINEAR
1K
260μf
VIBRATING REED RECORDER
OUT PUT 7.5 V
KEN TELL AMPLIFIER
OUT PUT 20 V
WESTON RECORDER
INPUT 100mv

Figure 8. Magnet current control

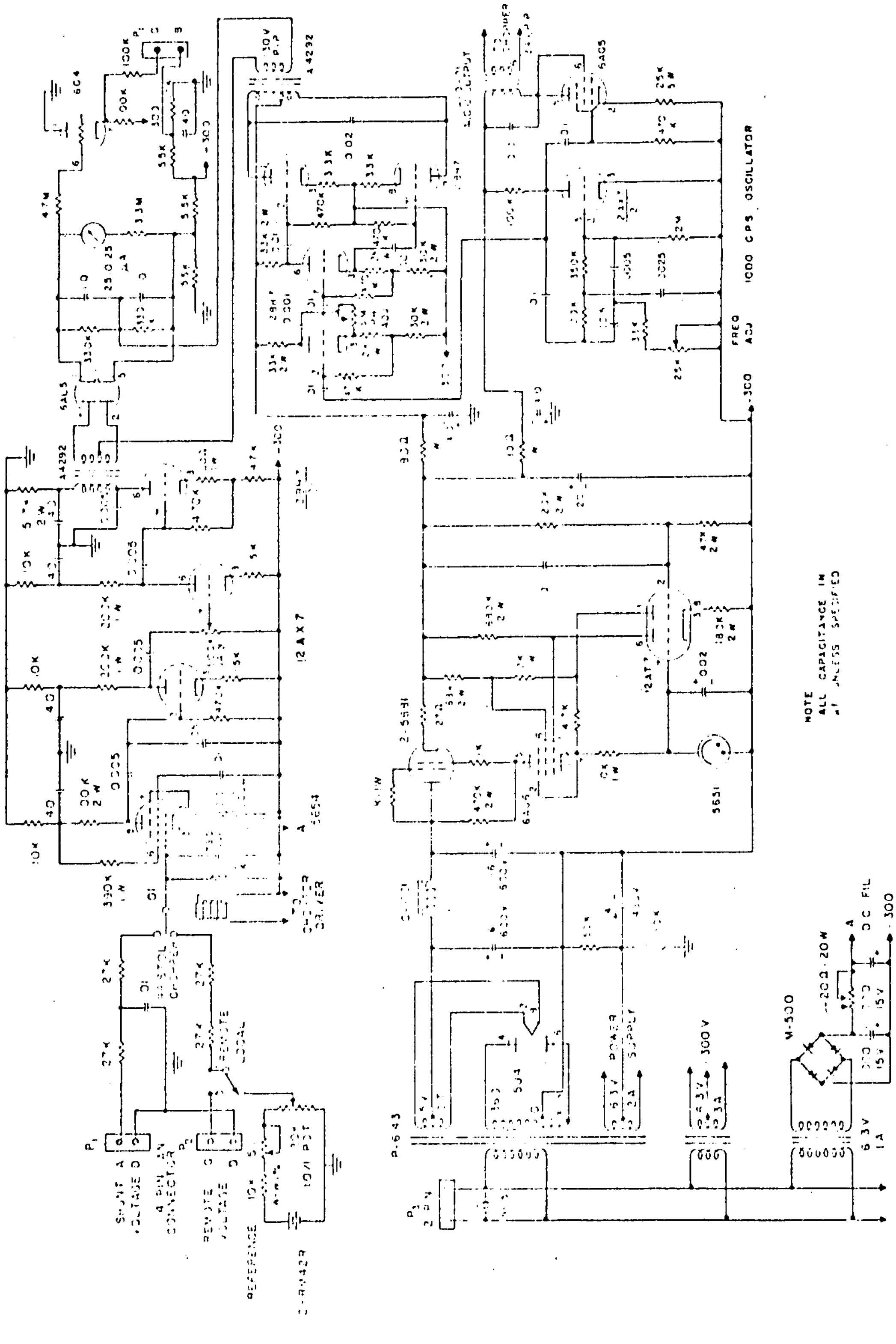

12AX7
1000 CPS OSCILLATOR
FREQ ADJ
POWER SUPPLY
300 V
M-500
6AG5
6AL5
6C4
5654
5651
NOTE ALL CAPACITANCE IN µF UNLESS SPECIFIED

Figure 9. Magnet power supply

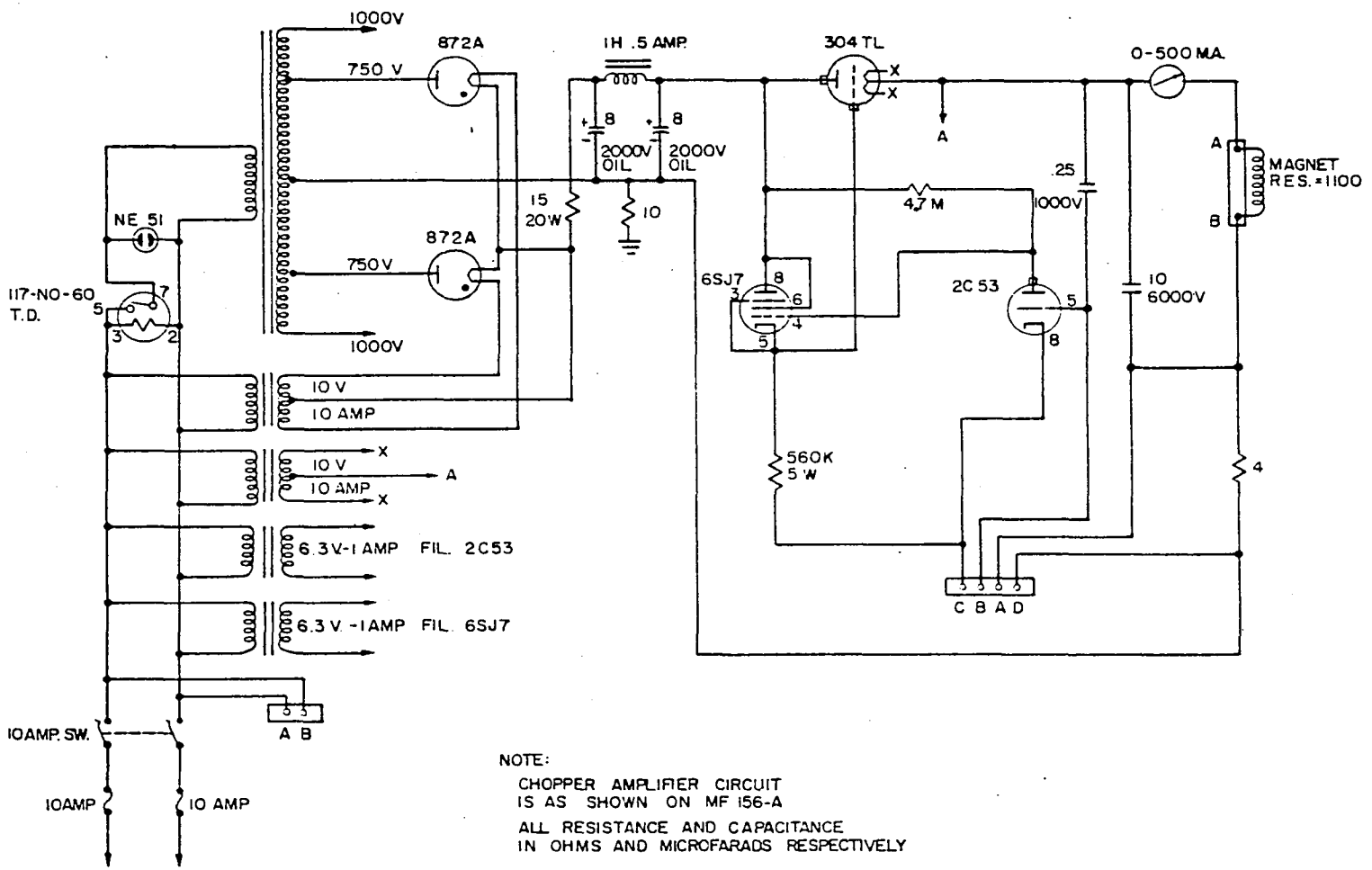

NOTE:

CHOPPER AMPLIFIER CIRCUIT IS AS SHOWN ON MF 156-A

ALL RESISTANCE AND CAPACITANCE IN OHMS AND MICROFARADS RESPECTIVELY

Figure 10. Cold cathode control circuit

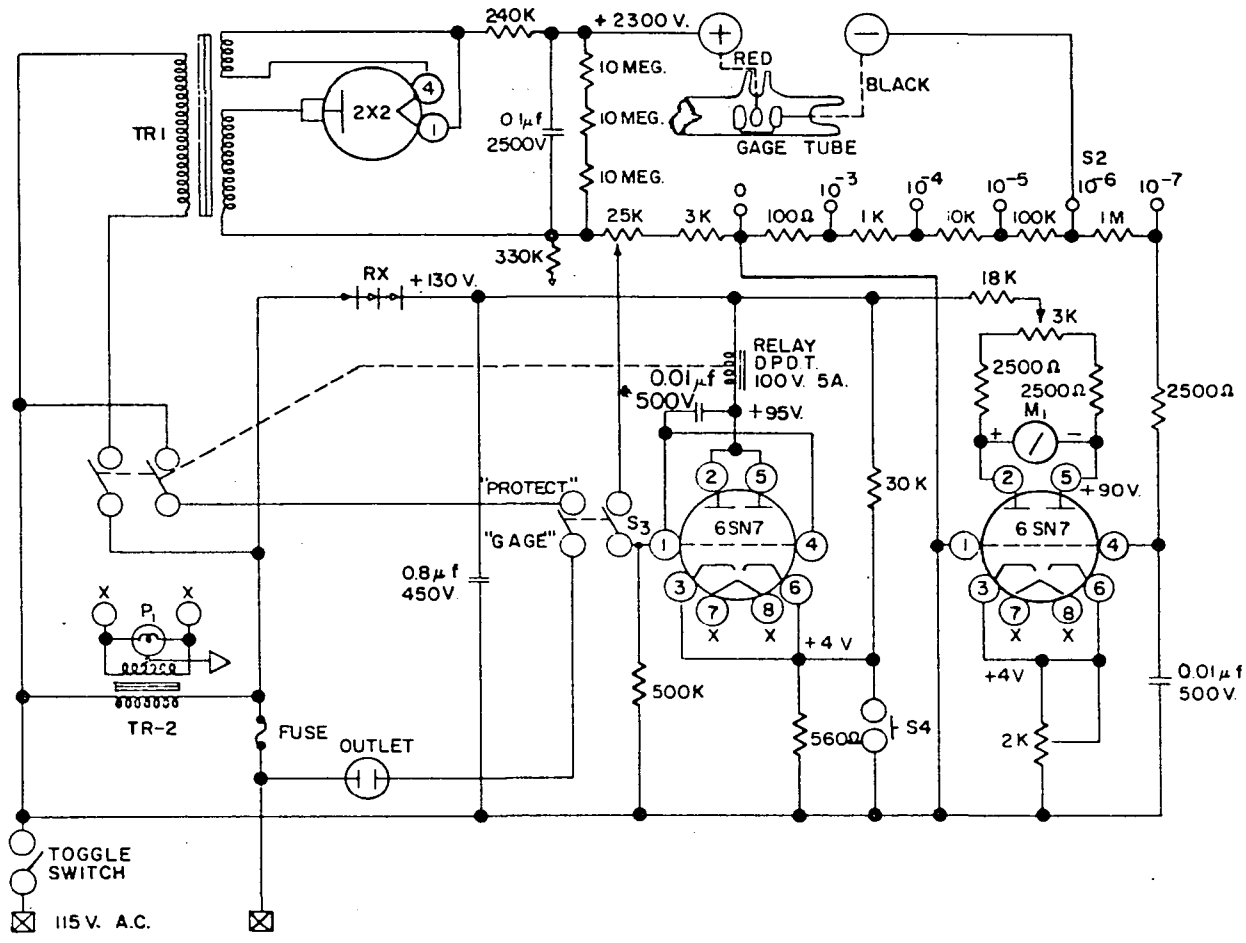
240K
+2300 V.
RED
BLACK
10 MEG.
10 MEG.
10 MEG.
GAGE TUBE
2X2
TR1
0.1μf
2500V
S2
0
10⁻³
10⁻⁴
10⁻⁵
10⁻⁶
10⁻⁷
25K
3K
100Ω
1K
10K
100K
1M
330K
RX
+130 V.
18K
3K
RELAY
DPDT
100V. 5A.
0.01μf
500V
+95V.
2500Ω
2500Ω
M1
2500Ω
"PROTECT"
"GAGE"
S3
6SN7
30K
+90V.
0.8μf
450V
X
P1
X
+4 V
+4V
500K
560Ω
S4
2K
0.01μf
500V.
TR-2
FUSE
OUTLET
TOGGLE
SWITCH
115 V. A.C.

II. SILANE

A. Introduction

The existence of silane was first demonstrated by Wöhler in 1857 when he dissolved aluminum containing silicon in hydrochloric acid. This reaction, however, gave very poor yields. The earliest method employed to prepare silane in quantities sufficient for the laboratory investigation of its properties was the hydrolysis of magnesium silicide, Mg_2Si, and other reactive-metal silicides. The gaseous product obtained by the above method is a mixture consisting of approximately 40 per cent SiH_4, 30 per cent Si_2H_6, 15 per cent Si_3H_8, 10 per cent Si_4H_{10} and 5 per cent higher hydrides (6). The yield obtained by this method is relatively low and the product is mixed with hydrogen. Better yields can be obtained by using concentrated phosphoric acid as the hydrolysis medium since hydrochloric acid hydrolyzes a large amount of silane. Yields can be improved further by carrying out the hydrolysis of magnesium silicide in liquid ammonia with ammonium bromide as the acidic reactant (7). One of the best preparations reported for monosilane is the metathetical reduction of silicon tetrachloride by means of lithium aluminum hydride in diethyl ether at zero degrees centigrade (8).

Silane is a colorless gas which explodes on exposure to

air. It is decomposed to silicon and hydrogen at a temperature of 600°C (6). The melting point of silane is -185°C, the boiling point is -111.8°C and density is 0.68 g/cc at -185°C (6). The heat of formation of monosilane has been reported to be 11.9 Kcal./mole by Hurd (6), 7.3 Kcal./mole by Gunn and Green (9) and -14.8 Kcal./mole by Rossini *et al.* (10). Silane has four hydrogen atoms arranged at the corners of a tetrahedron about the central silicon atom. Stevenson (11) predicts the Si-H spacing to be 1.49 A.U. and the bond angle at 109.5°. The silanes are strong reducing agents capable of precipitating a number of the heavier metals such as mercury and silver from solutions of their salts (6). A solution of potassium permanganate is reduced to brown manganese dioxide upon treatment with monosilane. Such a reduction may be used as a sensitive test for the presence of the silicon hydrides.

Reports of mass spectral studies of silane are rare. The only major publication on this hydride is that of Neuert and Clasen (12). Their results disagree with those found in this investigation and also with those reported by Frost[1] and the Callery Chemical Company[2]. The data

---

[1]Frost, D. C. Vancouver British Columbia. The mass spectrum of silane. Private communication (1959).

[2]Callery Chemical Company, Callery, Pennsylvania. The uncertified mass spectrum of silane. Private communication (1959).

presented by Neuert and Clasen appear to be in error by one mass unit due to their misidentification of the ion fragments. Also, the reported appearance potentials seem to include some excess kinetic energy when compared with the results found here.

B. Experimental

1. Preparation

Silane was prepared for this study by the method of Finholt et al. (8); i.e., by dropwise addition of 330 millimoles of silicon tetrachloride to a solution of 60 millimoles of lithium aluminum hydride in 50 milliliters of diethyl ether at zero degrees Centigrade. The reaction equation is

(1)

$$LiAlH_4 + SiCl_4 \xrightarrow[0^\circ C]{(C_2H_5)_2O} SiH_4 + LiCl + AlCl_3.$$

The reaction apparatus was swept with nitrogen throughout the addition of the silicon tetrachloride to the lithium aluminum hydride-ether slush. This addition took about thirty minutes. The gaseous products were swept first through a trap at -117°C (ethyl alcohol at its melting point) to remove the ether and higher silanes and then condensed in two traps in series and cooled with liquid nitrogen. The two nitrogen cooled traps then were isolated from the reaction vessel and the first trap allowed to warm to

-117°C, the crude silane distilling into the second liquid nitrogen trap. The second nitrogen trap was then isolated and allowed to warm to -117°C and the sample was collected by means of a hand operated Toepler pump. Mass spectrometric analysis of the gas collected showed it to be almost pure monosilane except for a trace impurity observed at mass 44. This peak was attributed to carbon dioxide. No dimer or higher silanes were observed in this sample.

2. Mass spectral properties

a. Fragmentation pattern The mass spectrum of silane is shown in Figure 11. This spectrum was obtained under the following conditions: ionizing current 95 microamperes; electron accelerating voltage 60 electron volts; ion accelerating voltage 1625 volts; and repeller voltage 1 volt. The relative peak heights of the fragments, corrected for change in pressure, are shown in Table 1. The relative peaks, calculated on the basis of the accepted isotope abundances (13) are shown in Table 2. As mentioned previously these results disagree with those of Neuert and Clasen (12). However, this mass scale was calibrated first from the known isotopes of nitrogen and then from oxygen by a method described elsewhere (14). Thus there can be no doubt about the validity of the mass scale. These results agree closely with those reported by Frost and the Callery Chemical Company.

Figure 11. The mass spectrum of silane

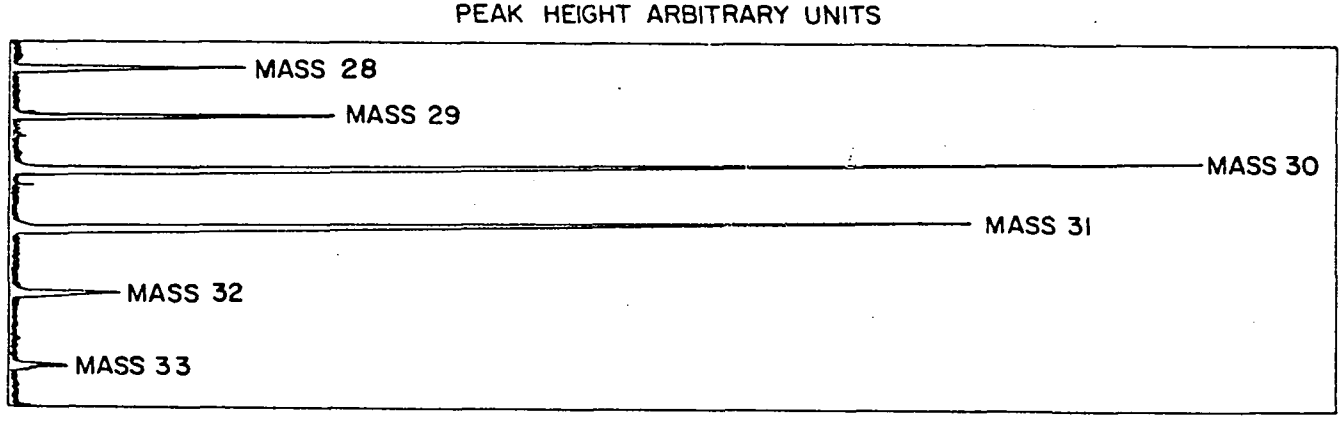
PEAK HEIGHT ARBITRARY UNITS
MASS 28
MASS 29
MASS 30
MASS 31
MASS 32
MASS 33

Table 1. Relative intensities and positive ion types of silane

Mass	Relative peak height	Positive ions		
28	20.3	$^{28}Si^+$		
29	21.0	$^{28}SiH^+$	$^{29}Si^+$	
30	100.0	$^{28}SiH_2^+$	$^{29}SiH^+$	$^{30}Si^+$
31	82.5	$^{28}SiH_3^+$	$^{29}SiH_2^+$	$^{30}SiH^+$
32	7.5	$^{28}SiH_4^+$	$^{29}SiH_3^+$	$^{30}SiH_2^+$
33	2.6		$^{29}SiH_4^+$	$^{30}SiH_3^+$
34	< 0.1			$^{30}SiH_4^+$

Table 2. Fragmentation pattern of silane

Silicon isotope	SiH_4^+	SiH_3^+	SiH_2^+	SiH^+	Si^+
28	< 1	78.1	100.0	20.3	20.7
29	< 1	78.1	100.0	20.3	20.8
30	< 1	78.0	100.0	20.3	20.7

b. Appearance potentials The manner and method of taking the data for the ionization efficiency plots have been fully described elsewhere (14). Extrapolation of the straight line portions of the ionization efficiency curves was the method (15) used for determining the values of the appearance potentials. While this method is admittedly subject to certain disadvantages, its simplicity was ideal and the values sufficient for the present study. The curves are shown in Figure 12 and the appearance potentials and their associated processes in Table 3. Since the SiH_4^+ peak was

Table 3. Appearance potentials and processes involved in the formation of the fragment ions from silane

Ion	Appearance potential	Process	
SiH_4^+	11.4 ± 0.3 ev (estimated)	$SiH_4 + e = SiH_4^+ + 2e$	(2)
SiH_3^+	11.8 ± 0.2	$SiH_4 + e = SiH_3^+ + H + 2e$	(3)
SiH_2^+	12.1 ± 0.2	$SiH_4 + e = SiH_2^+ + H_2 + 2e$	(4)
	16.5 ± 0.3	$SiH_4 + e = SiH_2^+ + 2H + 2e$	(5)
SiH^+	16.1 ± 0.2	$SiH_4 + e = SiH^+ + H_2 + H + 2e$	(6)
	20.4 ± 0.5	$SiH_4 + e = SiH^+ + 3H + 2e$	(7)
Si^+	11.7 ± 0.2	$SiH_4 + e = Si^+ + 2H_2 + 2e$	(8)
	16.4 ± 0.2	$SiH_4 + e = Si^+ + H_2 + 2H + 2e$	(9)
	20.8 ± 0.2	$SiH_4 + e = Si^+ + 4H + 2e$	(10)

Figure 12. Appearance potential curves of silane
Argon is used as an internal standard.

FROM SiH4
%pH RATIO
E A V (UNCORRECTED)

FROM SiH4
%pH RATIO
E A V (UNCORRECTED)

FROM SiH4
%pH RATIO
E A V (UNCORRECTED)

FROM SiH4
%pH RATIO
E A V (UNCORRECTED)

too small for a sensible measurement, its appearance potential was estimated in the same manner used for SnH_4^+ (14). While this method is tenuous, it allows one to obtain an estimate of the bond energies in the ion fragments. Errors cited in this thesis are estimated absolute errors and do not represent the reproducibility of the data.

If the appearance potential of Si^+ given in Equation 9 is combined with the heat of formation of Si^+ as given by Latimer (16), the standard heat of formation of SiH_4 can be calculated using Equation 11 (17).

$$\text{A.P. } (Si^+) = \Delta H_{reaction} = \Delta H_f^{\circ} (Si^+) + 2\ \Delta H_f^{\circ} (H_2) - \Delta H_f^{\circ} (SiH_4) + \text{K.E.} + \text{E.E.} \tag{11}$$

where A.P. = appearance potential

ΔH_f° = standard heat of formation

K.E. = excess kinetic energy - found to be negligible as described below

E.E. = excess excitation energy - assumed negligible.

This gives a value of 8.5 $\pm$ 4 Kcal./mole for $\Delta H_f^{\circ} (SiH_4)$ which closely agrees with the calorimetric value of 7.9 Kcal./mole reported by Gunn and Green (9). The appearance potential of 11.7 $\pm$ 0.2 electron volts for Si^+ is lower than the value of 14.5 $\pm$ 0.6 electron volts reported by Neuert and Clasen (12) for this fragment when their error in mass identification has been corrected. It is very possible that

their higher value contained excess kinetic energy. The average bond of the molecule can be calculated using Equation 12 (17) and the spectroscopic ionization potential of 8.15 electron volts (18).

$$\text{A.P.}\ (Si^+) = \text{I.P.}\ (Si) + 4\ \text{D.E.}(Si\text{-}H) - 2\ \text{D.E.}(H\text{-}H) + \text{K.E.} + \text{E.E.} \qquad (12)$$

where D.E. = bond dissociation energy

I.P. = ionization potential

All other terms are the same as in Equation 11.

The value of 72.2 $\pm$ 4 Kcal./mole obtained here agrees reasonably with the result of 76.5 Kcal./mole cited by Gunn and Green (9) and is in closer agreement with Cottrell's (19) value of 74.1 Kcal./mole.

Process 8 of Table 3 was examined for excess kinetic energy by the method of Taubert (5) and the results indicated no excess kinetic energy in the Si^+ fragment. For completeness this procedure will be described. The ion path, the focusing properties and the ion current collection efficiencies of a mass spectrometer depend on the geometry and the potentials of the various source electrodes as well as the initial velocity and starting point of the ion. Ion intensity is therefore dependent not only upon the ionization probability but also upon the initial energy. It is possible to obtain semi-quantitative information about these

energies from an investigation of relative ion intensities under varying ion source conditions. A change in the ion intensity depending on the initial energy can be produced simply by varying the ion repeller voltage. This method has an advantage over the procedure of Washburn and Berry (20) who vary the accelerating voltage in that only small readjustments of the magnetic field are necessary to refocus the ion beams.

Let E_R be the repeller voltage, I_x the ion intensity of the ion fragment under consideration and I_{th} the ion intensity of ions which have only thermal energy. Then if all the ions had the same initial conditions, there should be only a slight difference in relative ion intensities as a function of the mass number for different values of E_R. A plot of ion intensity against E_R is called the "characteristic of the ion source". In order to facilitate the comparison of the "characteristics" of I_x to I_{th}, the maxima of these curves are normalized to 100. The difference,

$$\Delta I_x (E_R) = I_x (E_R) - I_{th} (E_R), \qquad (13)$$

between the normalized characteristic of an ion X and the thermal ions likewise normalized for a certain repeller voltage E_R should be a measure of the kinetic energy. For silane, Si^+ was compared with Ar^+ at a repeller voltage of 1.0 volt just above their respective threshold potential and ΔI_{Si^+} was found to be zero. Thus, no kinetic energy was

present.

The bond energies of the various ion fragments may be calculated using the processes and equations summarized in Table 4. The values for the energies are given in Table 5.

Table 4. Processes and equations for determining the bond strengths of the ion fragments of silane

Process	Equation
$SiH_4 + e = SiH_4^+ + 2e$	$A.P._1 = I.P.(SiH_4) = 11.4$ e.v. (14)
$SiH_4 + e = SiH_3^+ + H + 2e$	$A.P._2 = A.P._1 + D.E.(SiH_3^+ - H) = 11.8$ (15)
$SiH_4 + e = SiH_2^+ + 2H + 2e$	$A.P._3 = A.P._2 + D.E.(SiH_2^+ - H) = 16.5$ (16)
$SiH_4 + e = SiH^+ + 3H + 2e$	$A.P._4 = A.P._3 + D.E.(SiH^+ - H) = 20.4$ (17)
$SiH_4 + e = Si^+ + 4H + 2e$	$A.P._5 = A.P._4 + D.E.(Si^+ - H) = 20.8$ (18)

Table 5. Dissociation energies of the various ion fragments of silane

Ion fragment	Dissociation energy
$SiH_3^+ - H$	0.4 e.v.
$SiH_2^+ - H$	4.7
$SiH^+ - H$	3.9
$Si^+ - H$	0.4

The low value for the bond dissociation energy in SiH_3^+-H supports the observation of a negligible amount of parent ions. The large values for the SiH_2^+-H and SiH^+-H bond energies are supported by the fragmentation pattern given in Table 2.

c. Cross-sections In order to compare such mass spectral data as fragmentation patterns of various gases, a knowledge of ionization cross-sections is necessary. These are difficult to measure absolutely but a convenient method of calculating them is that of Otvos and Stevenson (21) which will be described below.

Bethe (22) reports that the ionization cross-sections, $Q^i_{(n,\ell)}$ of an atomic electron, with quantum numbers (n,ℓ)

is approximately proportional to the mean square radius of the electron shell. Accordingly, Otvos and Stevenson (21) present evidence that the relative total ionization cross-sections of atoms are given, to a good approximation, by the weighted sum of the outer, or valence, electrons of the atoms where the weights are based on the mean square radii of the electron orbits. The relative total ionization cross-sections of molecules are the sum of the atomic cross-sections. To make the calculations let us start with the equation for the mean square radius of an electron with quantum number (n,ℓ) and a hydrogen-like wave function (23).

$$\bar{r}^2_{(n,\ell)} = \frac{a_o^2 \; n'^4}{(Z-S_{(n,\ell)})^2} \left[1 + \frac{3}{2}\left\{ 1 - \frac{\ell(\ell+1) - \frac{1}{3}}{n'^2} \right\} \right] \quad (19)$$

where $\bar{r}^2_{(n,\ell)}$ = mean square radius

a_o^2 = square radius of the Bohr orbit

l = azimuthal quantum number

n' = the effective quantum number

$S_{(n,\ )}$ = the screening constant

n' and $S_{(n,\ell)}$ are calculated by Slater's rules which are given by Eyring *et al.* (24). Equation 19 differs from the one given in Pauling and Wilson (23) in that Z has been changed to $Z-S_{(n,\ell)}$ to account for the screening of the

nucleus. This is known as the "effective nuclear charge". Also n, the regular quantum number, has been changed to n', "the effective quantum number". These quantities, n' and $S_{(n,\ell)}$ are used as adjustable constants which are varied so as to minimize the energy. Slater's rules are:

a. n' is assigned according to the value of the real quantum number n:

if n	=	1	2	3	4	5	6
then n'	=	1	2	3	3.7	4.0	4.2

b. For determining $S_{(n,\ell)}$ the electrons are divided into the following groups:

1s; 2s, 2p; 3s, 3p; 3d; 4s, 4p; 4d, 4f; ...

c. The shielding constant $S_{(n,\ell)}$ is formed for any group of electrons from the following contributions:

1. Nothing from any shell outside the one considered.

2. An amount 0.35 from each other electron in the group considered (except in the 1S group where 0.30 is used).

3. If a shell is an s or p, an amount 0.85 from each electron with principal quantum number less by 1, and an amount 1.00 from each electron still closer to the nucleus. If the shell is a d or f shell an amount 1.00 from each electron inside it.

Calculations: Define $Q^H = 1.00$. Si in the tetrahedral SiH_4 has Z = 14 and an electronic configuration of $1s^2 2s^2 2p^6 3s^1 3p^3$. If the electron in the 3s orbit is the one being considered, then:

orbits	$1s^2$	$2s^2 2p^6$	$3p^3 3s^1$
amount contributed to $S_{(n,\ell)}$	2 x 1.00	8 x 0.85	3 x 0.35

so $S_{(n,\ell)} = 2.00 + 6.80 + 1.05 = 9.85$

$Z - S_{(n,\ell)} = 14.00 - 9.85 = 4.15$ so $(Z-S)^2 = 17.22$

$n' = 3 \qquad n'^2 = 9 \qquad n'^4 = 81$

$$\bar{r}^2_{(3,1)} = \frac{81 a_0^2}{17.22}\left[1 + \frac{3}{2}\left\{1 - \frac{1(1+1) - \frac{1}{3}}{9}\right\}\right] = 10.45\ a_o^2$$

$$\bar{r}^2_{(3,0)} = \frac{81 a_0^2}{17.22}\left[1 + \frac{3}{2}\left\{1 - \frac{0(0+1) - \frac{1}{3}}{9}\right\}\right] = 12.02\ a_o^2$$

for H $n' = 1 \qquad Z = 1 \qquad S_{(1,0)} = 0$

$$\bar{r}^2_{(1,0)} = \frac{a_o^2}{1}\left[1 + \frac{3}{2}\left\{1 - \frac{0(0+1) - \frac{1}{3}}{1}\right\}\right] = 3\ a_o^2$$

$$\frac{Q^H}{Q^{Si}} = \frac{(\text{valence electrons})\ (r^2_{(1,0)})}{(\text{valence electrons of 3s})\ (r^2_{(3,0)}) + (\text{valence electrons of 3p})(r^2_{(3,1)})}$$

$$\frac{1.00}{Q^{Si}} = \frac{(1)\ (3)\ a_o^2}{(1 \times 12.02) + 3(10.45)\ a_o^2} = \frac{3}{43.37}$$

$$Q^{Si} = 14.4$$

$$Q^{SiH_4} = 14.4 + 4(1) = 18.4.$$

The cross-section values will be used in the appendices where a comparison of the fragmentation patterns of the hydrides in this study will be made.

III. GERMANE

A. Introduction

In 1902 Voegelen discovered that when zinc reacts with sulfuric acid containing germanium, the hydrogen evolved contained some germanium hydride (25). In 1924 Dennis *et al.* (26) found that dilute sulfuric acid reacting with Mg_2Ge gave not only monogermane, GeH_4, but also digermane, Ge_2H_6, and trigermane, Ge_3H_8. They also reported the formation of a solid hydride, Ge_yH_x, in this reaction. The hydrolysis of Mg_2Ge by dilute hydrochloric acid is said to give yields of 20 to 25 per cent GeH_4 (6). Another preparation for GeH_4 is that of Finholt *et al.* (8) which was described in chapter II. This lithium aluminum hydride reduction of germanium tetrachloride has been reported to give unsatisfactory yields by Sujishi and Keith (27). These investigators claim the reduction of the tetrachloride with lithium tri-t-butoxyaluminohydride to be superior. Recent publications by Macklen (28), Piper and Wilson (29), Jolly (30), and Jolly and Drake (31) fully discuss the formation of the germanes by the reduction of germanium IV compounds with aqueous borohydride solutions.

Germane is a regular tetrahedron with a Ge-H bond distance of 1.37 A.U. according to Steward and Nielsen (32). Stevenson (11) calculates the bond length to be 1.54 A.U.

and the bond angle 109.5°. A value of 21.6 Kcal./mole has been given by Gunn and Green (9) for the heat of formation. Some physical properties of the germanes are listed in Table 6 (6).

Monogermane is not spontaneously inflammable in air as is silane. This has been attributed however to the greater strength of the Si-O bond rather than to silane being less stable than germane. Indeed, heat of formation measurements show silane to be the more stable. Germane is a strong reducing agent and will precipitate free metal from such solutions as silver nitrate (6). It will decompose to germanium and hydrogen at 350°C and if ignited directly will burn to water and germanium dioxide. Jolly and Drake (31) report that germane may be stored in a glass vessel with a greased stopcock. Such stability was observed in this

Table 6. Physical properties of the germanes

	GeH_4	Ge_2H_6	Ge_3H_8
Melting point	-165° C	-109° C	-105.6° C
Boiling point	-88.5° C	29° C	110.5° C
Density	1.523 g/cc at -142° C	1.98 g/cc at -109° C	ca. 2.2 g/cc at 20° C

investigation. Gunn and Green (9) report that it has been stored in a blackened flask at room temperature for two years with little decomposition.

There are two mass spectral reports on germane. One by Neuert and Clasen (12) who again are one mass unit low in the calibration of their mass scale and the second by de Mévergnies and Delfosse (33) whose fragmentation patterns concur with the results found in this work.

B. Experimental

1. Preparation

Germane, digermane and trigermane were prepared by the method of Jolly and Drake (31). Their report furnished many missing details to a similar study that was underway in these laboratories at the time of its publication. Germane and digermane were prepared by the dropwise addition of a ten milliliter solution containing 0.1 gram of germanium dioxide, 0.15 gram of potassium borohydride and 0.2 gram of potassium hydroxide to 12 milliliters of glacial acetic acid over a period of ten minutes. The products were swept from the reaction flask through a trap at -63.5° C (chloroform at its melting point) to remove trigermane, water and acetic acid. Next the gases were passed through tubes containing ascarite and magnesium perchlorate to remove the carbon dioxide and dry the gases further. Finally the gases were

condensed in two liquid-nitrogen-cooled traps. The reaction equations are

$$HGeO_3^- + BH_4^- + 2\ H^+ = GeH_4 + H_3\ BO_3 \qquad (20)$$

$$8\ H\ GeO_3^- + 7\ BH_4^- + 15\ H^+ = 4\ Ge_2H_6 + 7\ H_3BO_3 + 3\ H_2O. \qquad (21)$$

The digermane and germane were separated by distilling the products through a carbon disulfide slush bath (-111.6°C). Sanderson (34) fully discusses the general vacuum techniques used for this separation. The products collected were then analyzed in the mass spectrometer and it was observed that monogermane and digermane were completely separated. Since germanium has five naturally occurring isotopes, the mass spectrum was quite complex. Using a separated isotope greatly simplified the germane spectrum. Unfortunately, the price of this isotope, germanium 74, was too high to justify its use in a separate preparation of trigermane. Trigermane was prepared, in better yields than were obtained in the above reaction, by the dropwise addition of a 25 milliliter solution containing 1 gram of germanium dioxide, 2.1 grams of sodium borohydride, and 2 grams of 85 per cent potassium hydroxide to 120 milliliters of 3 molar sulfuric acid over a period of 20 minutes. The reaction equation is:

$$6\ H\ GeO_3^- + 5\ BH_4^- + 11\ H^+ = 2\ Ge_3H_8 + 5\ H_3BO_3 + 3\ H_2O. \quad (22)$$

For this preparation, mass spectral analyses showed complete separation of monogermane and digermane, but digermane and trigermane were not completely separated. This was no serious handicap since the fragmentation pattern of trigermane could still be obtained without interference. The fragmentation patterns of the monomer and dimer were obtained from the first preparation. In both these preparations a small amount of a yellow substance was observed in the reaction flask. This has been reported to be a polymeric germanium hydride GeH_x where $x \simeq 1.0$ by Jolly and Drake (31).

2. Mass spectral properties

a. Fragmentation pattern The mass spectrum of monogermane is shown in Figure 13. The spectrum was obtained with the similar conditions prevailing in the ion source as described for silane on page 34. The relative intensities of the peak heights of the spectrum, corrected for change in pressure and flow rate, are shown in Table 7 and the fragmentation patterns calculated from the known isotope abundances (13) are shown in Table 8. As was the case with silane, these results disagree with those of Neuert and Clasen (12). The mass scale for germane in this investigation was checked by the isotopes of both molecular

Figure 13. The mass spectrum of monogermane prepared from natural germanium

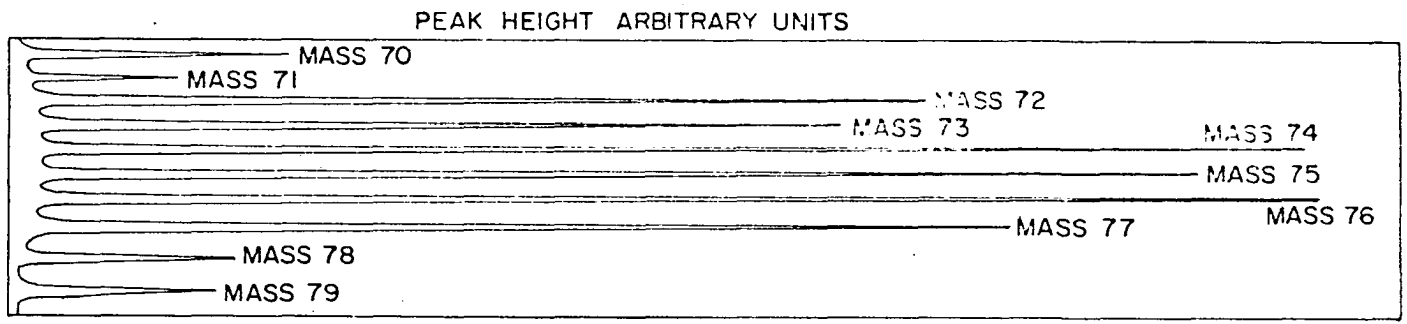
PEAK HEIGHT ARBITRARY UNITS
MASS 70
MASS 71
MASS 72
MASS 73
MASS 74
MASS 75
MASS 76
MASS 77
MASS 78
MASS 79

chlorine and krypton so there can be no doubt about its correctness. The fragmentation pattern reported here agrees reasonably well with that of de Mévergnies and Delfosse (33).

Table 7. Relative ion intensities of the mass spectrum and positive ion types of monogermane prepared from naturally abundant germanium

Mass	Relative peak height	Positive ions				
70	21.2	$^{70}GeH^+$				
71	12.0	$^{70}GeH^+$				
72	72.9	$^{70}GeH_2^+$	$^{72}Ge^+$			
73	64.6	$^{70}GeH_3^+$	$^{72}GeH^+$	$^{73}Ge^+$		
74	100.0	$^{70}GeH_4^+$	$^{72}GeH_2^+$	$^{73}GeH^+$	$^{74}Ge^+$	
75	93.6		$^{72}GeH_3^+$	$^{73}GeH_2^+$	$^{74}GeH^+$	
76	91.5		$^{72}GeH_4^+$	$^{73}GeH_3^+$	$^{74}GeH_2^+$	$^{76}Ge^+$
77	80.6			$^{73}GeH_4^+$	$^{74}GeH_3^+$	$^{76}GeH^+$
78	17.5				$^{74}GeH_4^+$	$^{76}GeH_2^+$
79	20.2					$^{76}GeH_3^+$
80	< 1.0					$^{76}GeH_4^+$

Table 8. Fragmentation pattern of monogermane prepared from naturally abundant germanium

Germanium isotope	GeH_4^+	GeH_3^+	GeH_2^+	GeH^+	Ge^+
70	< 0.5	91.0	100.0	26.9	47.5
72	< 0.5	91.0	100.0	26.9	47.5
73	< 0.5	90.6	100.0	26.9	47.3
74	< 0.5	91.2	100.0	26.9	47.5
76	< 0.5	90.6	100.0	26.9	47.3

Germane was prepared from germanium-74 dioxide and the spectrum rerun. This spectrum is shown in Figure 14 and the fragmentation pattern is given in Table 9. In this case the mass scale was calibrated with molecular chlorine.

Digermane, prepared from naturally abundant germanium, was analyzed in the mass spectrometer and the spectrum is shown in Figure 15. The ion intensities are listed in Table 10. The conditions in the ion source were the same as those given previously on page 34.

The 105 types of positive ions are too numerous to list in the above table. Using the known isotope abundances the fragmentation pattern was calculated and is listed in Table 11.

Figure 14. Mass spectrum of monogermane prepared from germanium-74 dioxide

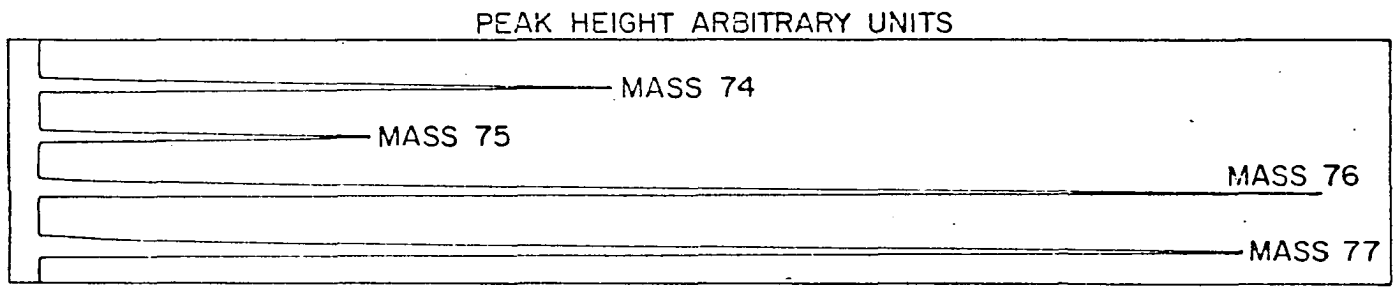
PEAK HEIGHT ARBITRARY UNITS
MASS 74
MASS 75
MASS 76
MASS 77

Figure 15. Mass spectrum of digermane prepared from naturally abundant germanium

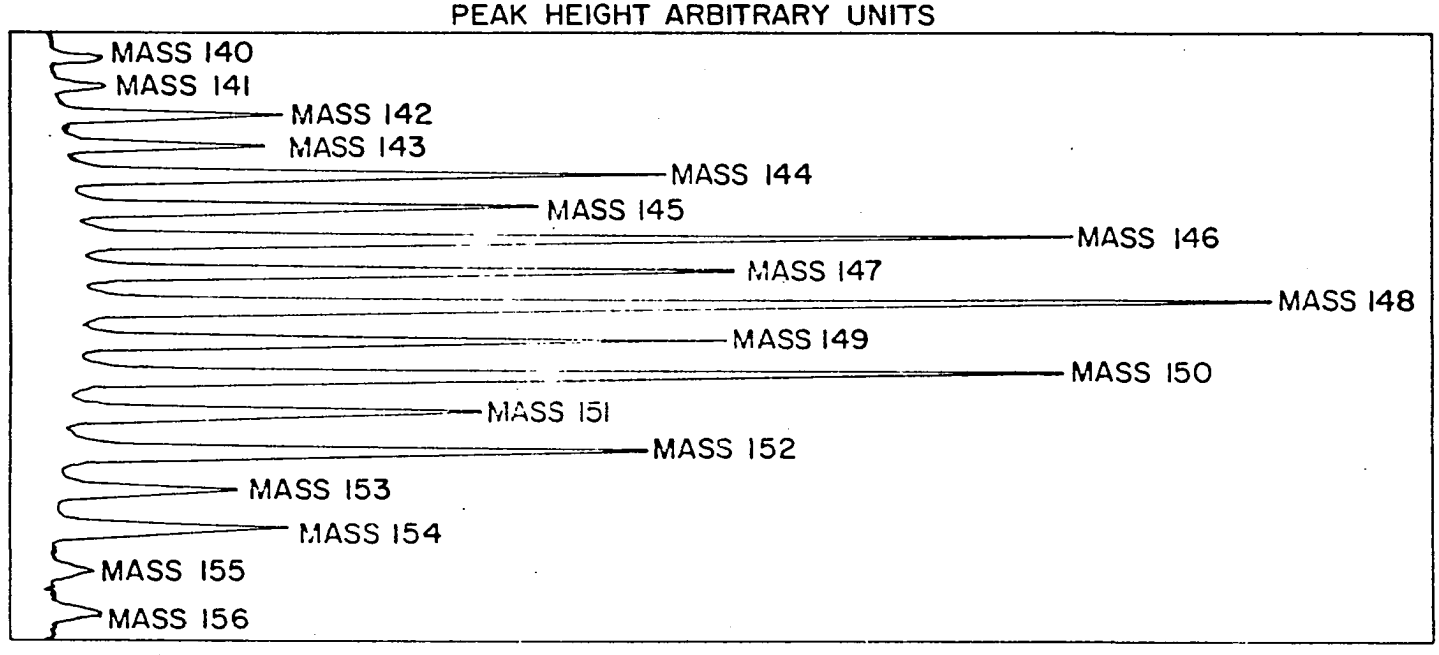
PEAK HEIGHT ARBITRARY UNITS
MASS 140
MASS 141
MASS 142
MASS 143
MASS 144
MASS 145
MASS 146
MASS 147
MASS 148
MASS 149
MASS 150
MASS 151
MASS 152
MASS 153
MASS 154
MASS 155
MASS 156

Table 9. Fragmentation pattern of monogermane prepared from germanium-74 dioxide

Fragment	Relative peak height
$^{74}GeH_4^+$	< 0.5
$^{74}GeH_3^+$	93.7
$^{74}GeH_2^+$	100.0
$^{74}GeH^+$	28.3
$^{74}Ge^+$	47.5

Table 10. Relative ion intensities of digermane prepared from naturally abundant germanium

Mass	Relative peak height
140	4.8
141	4.9
142	20.0
143	18.9
144	62.0
145	48.0
146	100.0
147	68.8

Table 10 (Continued).

Mass	Relative peak height
148	99.4
149	44.4
150	66.4
151	25.7
152	40.7
153	11.1
154	14.7
155	3.0
156	4.4
157	0.3
158	0.4

Table 11. Fragmentation pattern of digermane prepared from normal germanium

Ion fragment:	Ge_2^+	Ge_2H^+	$Ge_2H_2^+$	$Ge_2H_3^+$	$Ge_2H_4^+$	$Ge_2H_5^+$	$Ge_2H_6^+$
Relative peak height :	56	66	100	25	66	25	43

Digermane, prepared from germanium-74 dioxide, gave the mass spectrum shown in Figure 16 and the fragmentation pattern listed in Table 12.

Table 12. Fragmentation pattern of digermane prepared from germanium-74 dioxide

Mass	Ion types	Relative peak height
154	$^{74}Ge_2H_6^+$	43.0
153	$^{74}Ge_2H_5^+$	25.2
152	$^{74}Ge_2H_4^+$	68.6
151	$^{74}Ge_2H_3^+$	28.3
150	$^{74}Ge_2H_2^+$	100.0
149	$^{74}Ge_2H^+$	60.4
148	$^{74}Ge_2^+$	63.0
78	$^{74}GeH_4^+$	5.4
77	$^{74}GeH_3^+$	32.1
76	$^{74}GeH_2^+$	34.5
75	$^{74}GeH^+$	11.8
74	$^{74}Ge^+$	41.2

Figure 16. Mass spectrum of digermane prepared from germanium-74 dioxide

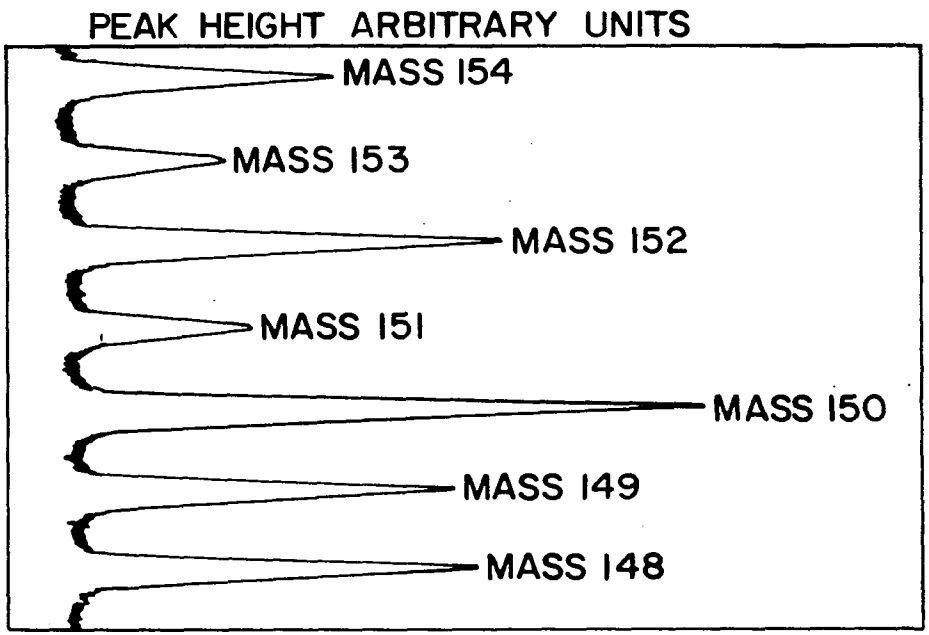
PEAK HEIGHT ARBITRARY UNITS
MASS 154
MASS 153
MASS 152
MASS 151
MASS 150
MASS 149
MASS 148

Because of larger peaks obtained in the separated isotope preparation, this data is considered more reliable. It should be noted that GeH_4^+ was observed in the dimer spectrum while it was not observed in the monomer. Since this peak height varied proportionately as the square root of the pressure, its presence was attributed to a secondary process occurring in the ion source. The mass scale for digermane was calibrated with chromyl chloride which was prepared by the method of Flesch and Svec (35) who also characterized the mass spectrum of this compound (36).

Trigermane's mass spectrum was analyzed on the mass spectrometer described by Flesch and Svec (36) before the building of the present instrument was completed. It was not reanalyzed on the instrument described in this report because it was felt that the data previously taken was sufficient for this present study since there was insufficient germanium-74 for a separate trigermane preparation. The mass spectrum of trigermane is shown in Figure 17 and the fragmentation pattern calculated from known isotopic abundances in Table 13. The ion source conditions in this instrument have been published elsewhere (36,37). Due to the large number, 315, of ion fragments formed from trigermane, the calculation of the fragmentation pattern must be considered tenuous. It was not possible to positively calibrate the mass scale in this high mass range.

Figure 17. Mass spectrum of trigermane prepared from naturally abundant germanium

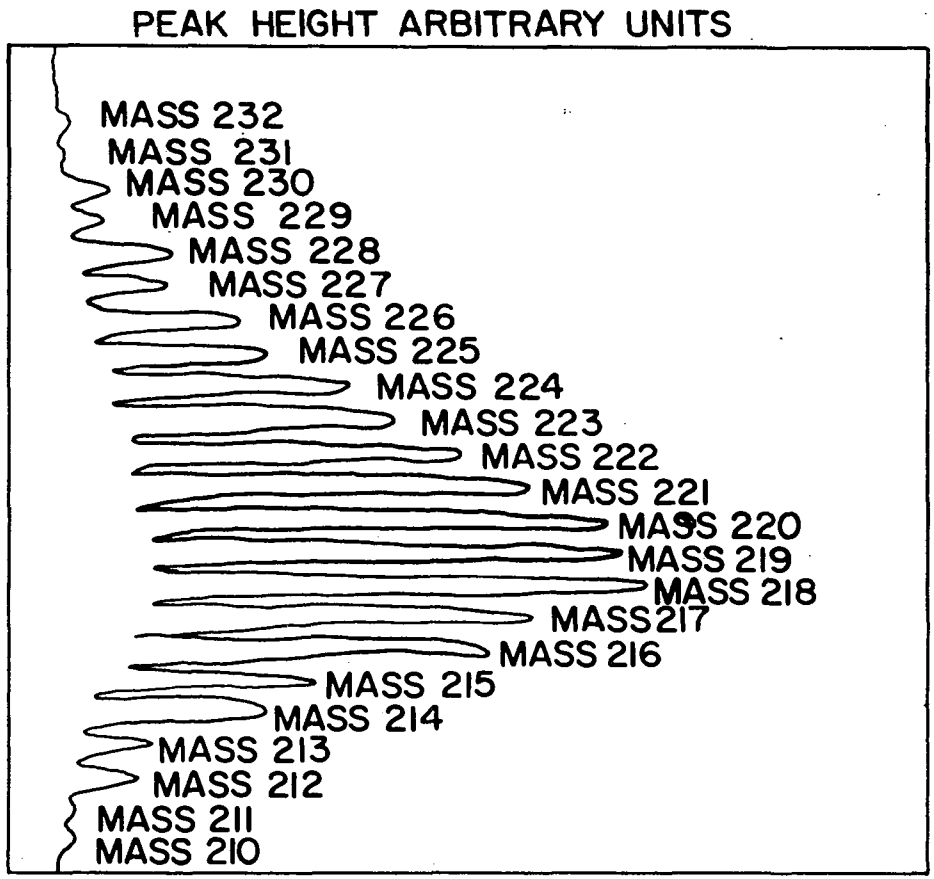
PEAK HEIGHT ARBITRARY UNITS
MASS 232
MASS 231
MASS 230
MASS 229
MASS 228
MASS 227
MASS 226
MASS 225
MASS 224
MASS 223
MASS 222
MASS 221
MASS 220
MASS 219
MASS 218
MASS 217
MASS 216
MASS 215
MASS 214
MASS 213
MASS 212
MASS 211
MASS 210

Table 13. Fragmentation pattern of trigermane prepared from naturally abundant germanium

Ion fragment	Relative ion current
$Ge_3H_8^+$	26
$Ge_3H_7^+$	16
$Ge_3H_6^+$	3
$Ge_3H_5^+$	3
$Ge_3H_4^+$	12
$Ge_3H_3^+$	12
$Ge_3H_2^+$	5
Ge_3H^+	100
Ge_3^+	100

b. Appearance potentials The same manner and method of taking appearance potential data were used for germane as were used for silane (14). The ionization efficiency curves are shown in Figure 18 and the appearance potentials and associated processes in Table 14. Krypton was used as an internal standard to calibrate the voltage scale. The appearance potentials are reported only for the

Figure 18. Ionization efficiency curves for the fragments of germane prepared from germanium-74 dioxide

Krypton is used as an internal standard.

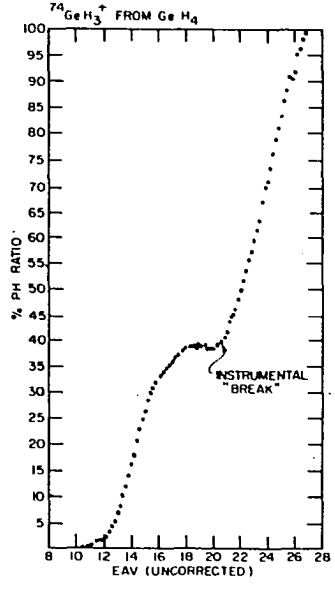
$^{74}GeH_3^+$ FROM GeH_4
% PH RATIO
EAV (UNCORRECTED)
INSTRUMENTAL "BREAK"

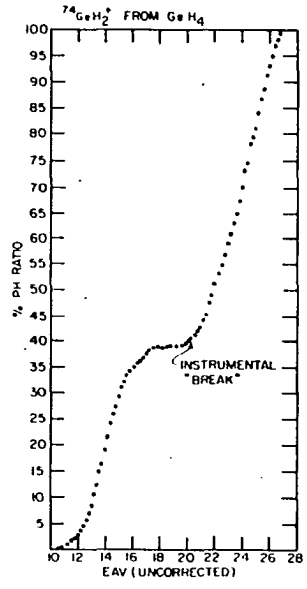
$^{74}GeH_2^+$ FROM GeH_4
% PH RATIO
EAV (UNCORRECTED)
INSTRUMENTAL "BREAK"

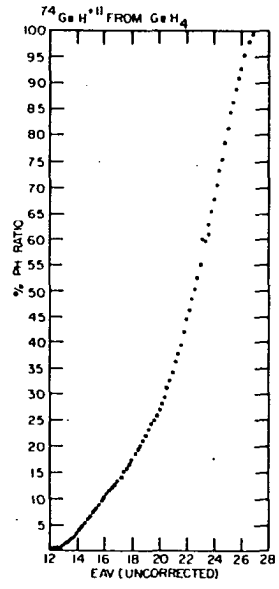
$^{74}GeH^{+11}$ FROM GeH_4
% PH RATIO
EAV (UNCORRECTED)

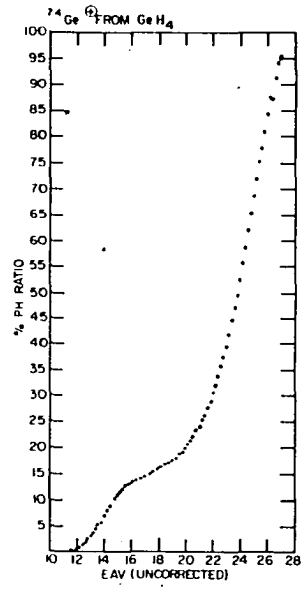
$^{74}Ge^{+12}$ FROM GeH_4
% PH RATIO
EAV (UNCORRECTED)

Table 14. Appearance potentials and processes involved in the formation of the fragments from germane prepared from germanium-74 dioxide

Ion	Appearance potential	Process	
$^{74}GeH_4^+$	10.5 ± 0.3 e.v. (estimated)	$GeH_4 + e = GeH_4^+ + 2e$	(23)
$^{74}GeH_3^+$	10.8 ± 0.3	$GeH_4 + e = GeH_3^+ + H + 2e$	(24)
$^{74}GeH_2^+$	11.0 ± 0.2	$GeH_4 + e = GeH_2^+ + H_2 + 2e$	(25)
	15.4 ± 0.3	$GeH_4 + e = GeH_2^+ + 2H + 2e$	(26)
$^{74}GeH^+$	11.3 ± 0.2	$GeH_4 + e = GeH^+ + H_2 + H + 2e$	(27)
	16.8 ± 0.3	$GeH_4 + e = GeH^+ + 3H + 2e$	(28)
$^{74}Ge^+$	10.7 ± 0.2	$GeH_4 + e = Ge^+ + 2H_2 + 2e$	(29)
	14.1 ± 0.5	$GeH_4 + e = Ge^+ + H_2 + 2H + 2e$	(30)
	18.3 ± 0.3	$GeH_4 + e = Ge^+ + 4H + 2e$	(31)

fragments from germane which had been prepared from the separated isotope. Once again the parent ion, GeH_4^+, was too small for a sensible measurement, so its appearance potential was estimated in the same manner used for SiH_4^+ and SnH_4^+.

If the appearance potential of Ge^+ given in Equation 29 is combined with the heat of formation of Ge^+ (16) and used in Equation 11, a value of 20.8 $\pm$ 4 Kcal./mole is obtained for the heat of formation of germane. This agrees well with the value of 21.6 Kcal./mole cited by Gunn and Green (9). The values for the appearance potentials of the fragments are lower than the values given by Neuert and Clasen and by de Mévergnies and Delfosse. One possible explanation for the different values is the fragments reported by those authors may contain excess kinetic energy. Another explanation could be that these authors misinterpreted the process occurring in the ion source. In this work, only the Ge^+ fragment was tested for kinetic energy by Taubert's method (5) which was described in chapter II. Since no kinetic energy was found in the Ge^+ fragment and the energy is inversely proportional to the mass, the higher mass fragments were also assumed to contain no kinetic energy. When the appearance potential given in Equation 29 is combined with the spectroscopic ionization potential of 7.88 electron volts as cited by Moore (38) and used in Equation 12, an

energy of 68.3 ± 4 Kcal./mole is found for the average Ge-H bond. This concurs with the value of 69.0 Kcal./mole reported by Gunn and Green. The bond energies of the various ion fragments may also be calculated using the processes and equations listed in Table 15. The bond energies of the ion fragments are cited in Table 16.

The low value for the GeH_3^+-H bond supports the fact that a negligible amount of parent ion was observed. It is not apparent why the GeH_2^+ ion is more abundant than the GeH_3^+ ion in view of the bond energies given below. A possible explanation for the discrepancy is a misinterpretation of the processes occurring in the ion source. This is reasonable since the values of the various processes listed in Table 14, in which a hydrogen bond is formed, differ from the accepted value of the hydrogen bond energy.

c. Cross-sections The relative ionization cross-section of germane, calculated by the method of Otvos and Stevenson (21) which was discussed in chapter II, is 22.4.

Table 15. Processes and equations for determining the bond strengths of the ion fragments of germane prepared from germanium-74 dioxide

Process	Equation
$GeH_4 + e = GeH_4^+ + 2e$	$A.P._1 = I.P.\ (GeH_4) = 10.5$ e.v. (32)
$GeH_4 + e = GeH_3^+ + H + 2e$	$A.P._2 = A.P._1 + D.E.(GeH_3^+-H) = 10.8$ (33)
$GeH_4 + e = GeH_2^+ + 2H + 2e$	$A.P._3 = A.P._2 + D.E.(GeH_2^+-H) = 15.4$ (34)
$GeH_4 + e = GeH^+ + 3H + 2e$	$A.P._4 = A.P._3 + D.E.(GeH^+-H) = 16.8$ (35)
$GeH_4 + e = Ge^+ + 4H + 2e$	$A.P._5 = A.P._4 + D.E.(Ge^+-H) = 18.3$ (36)

Table 16. Dissociation energies of the various ion fragments of germane

Ion fragment	Dissociation energy
GeH_3^+-H	0.3 e.v.
GeH_2^+-H	4.6
GeH^+-H	1.4
Ge^+-H	1.5

IV. STANNANE

The results for stannane have been published elsewhere (14,37) and will be summarized here for completeness. The standard heat of formation of stannane was calculated from the above data and found to be 23.0 ± 4 Kcal./mole which is lower than the value of 38.9 Kcal./mole reported by Gunn and Green. This difference may be reasonably explained by the presence of excess kinetic energy in the Sn^+ fragment. With the instrument used in the stannane study there was no way to detect this energy. The average Sn-H bond energy was found to be 70.3 ± 4 Kcal./mole using Equation 45 and the spectroscopic ionization potential. This value is higher than the bond energy of 60.4 Kcal./mole given by Gunn and Green (9) but concurs with the infrared value of 73.7 Kcal./mole given by May and Dillard (39) and with the theoretical value of 71 Kcal./mole calculated by Huggins (40). The appearance potentials and their processes are listed in Table 17, the ion fragment bond energies in Table 18, and the fragmentation pattern in Table 19. The relative ionization cross-section of stannane as calculated from the work of Otvos and Stevenson (21) is 29.8.

While no dimer was observed in the above work, Jolly (41) has reported its existence. In a subsequent paper he has characterized this hydride further (30,31). All attempts to repeat his synthesis and to introduce distannane

Table 17. Appearance potentials and processes involved in the formation of the fragment ions from stannane prepared from tin 120

Ion	Appearance potential	Process	
SnH_4^+	11.7 ± 0.3 e.v. (estimated)	$SnH_4 + e = SnH_4^+ + 2e$	(37)
SnH_3^+	11.9 ± 0.2	$SnH_4 + e = SnH_3^+ + H + 2e$	(38)
SnH_2^+	12.1 ± 0.2	$SnH_4 + e = SnH_2^+ + H_2 + 2e$	(39)
	16.4 ± 0.3	$SnH_4 + e = SnH_2^+ + 2H + 2e$	(40)
SnH^+	13.3 ± 0.2	$SnH_4 + e = SnH^+ + H_2 + H + 2e$	(41)
	17.3 ± 0.5	$SnH_4 + e = SnH^+ + 3H + 2e$	(42)
Sn^+	11.4 ± 0.2	$SnH_4 + e = Sn^+ + 2H_2 + 2e$	(43)
	15.5 ± 0.2	$SnH_4 + e = Sn^+ + H_2 + 2H + 2e$	(44)
	19.5 ± 0.2	$SnH_4 + e = Sn^+ + 4H + 2e$	(45)

Table 18. Bond energies of the ion fragments of stannane prepared from tin 120

Ion	Bond energy
SnH_3^+-H	0.2 e.v.
SnH_2^+-H	4.5
SnH^+-H	0.9
Sn^+-H	2.2

Table 19. Fragmentation patterns of SnH_4 prepared from the separated isotope tin 120

Ion	Relative peak height
SnH_4^+	< 0.1
SnH_3^+	100.0
SnH_2^+	53.6
SnH^+	21.5
Sn^+	70.6

into the mass spectrometer failed. This may be attributed to the instability of distannane at room temperature. A metallic mirror, found on the glass tube leading into the ionization chamber which had been cleaned before the attempted introduction of distannane, was shown to be tin by a spot test (42). A mirror was also formed in the cold trap where the distannane and stannane were originally frozen when this trap was warmed to room temperature. Such a mirror could not have been formed from stannane because the tube had been evacuated at -63.5° C (chloroform at its melting point) where stannane is in the gaseous state before the tube had been allowed to warm. This mirror also gave a tin

test. The observed instability of distannane corroborates the findings of Jolly and Drake (31).

V. PLUMBANE

A. Introduction

Plumbane is more unstable than any of the other hydrides in group IVB. It has been claimed (43) that PbH_4 decomposes to lead and hydrogen at 0° C. Paneth and Nörring (44) first prepared plumbane by electrolyzing a sulfuric acid solution with a lead electrode. The gas was identified by radio active tracer methods (45). Paneth (45) claimed in 1928 that it would only be a question of time until the properties of plumbane would be reported. Thirty years have added little to the knowledge of this hydride. Plumbane may also be prepared by the action of acids on a mixture of magnesium and lead pellets and by the reduction of a dilute solution of lead acetate with metallic magnesium. Kramer (46) claims that sodium borohydride is thermodynamically incapable of reducing lead nitrate to plumbane and Jolly (30) states that if plumbane is formed from this reaction, it immediately decomposes to the elements. Both of these investigators claim that metallic lead is formed in the reaction. This fact was observed here.

B. Experimental

Two different methods of preparing plumbane were attempted without success. In the first 0.5 millimole of lead nitrate was dissolved in 50 milliliters of water. This

solution was then made acidic by the addition of 2.5 milliliters of concentrated hydrochloric acid and was added over a period of 15 minutes to a 10 per cent aqueous solution of sodium borohydride. When the gases were collected and analyzed on the mass spectrometer no PbH_4 was observed. The second preparation attempted was the reduction of lead acetate with metallic magnesium. The results of this preparation were also negative.

VI. PHOSPHINE

A. Introduction

Phosphine was discovered in 1783 by Gengembre who heated while phosphorus with alkali (47). When crude calcium phosphide is treated with water, a gas, spontaneously inflammable in air, is formed. If pure calcium phosphide is used the product does not spontaneously ignite according to Moissan's findings in 1899 (47). The spontaneous flammability was shown by Thenard in 1844 to be due to a small amount of diphosphine (47). Recently, Addison and Plummer (48) have shown that it is possible to obtain spectroscopically pure phosphine from the hydrolysis of calcium phosphide. They removed diphosphine by fractional distillation and acetylene by allowing the gas to stand over a molecular sieve at 100° C for 12 hours. The reduction of phosphorus trichloride with lithium aluminum hydride has been discussed by Paddock (49) and is a satisfactory preparation of phosphine.

Phosphine is a colorless, poisonous gas with a very unpleasant odor. Some physical properties of phosphine, as cited by Hurd (6), are listed in Table 20.

Gunn and Green (9) report 1.3 Kcal./mole for the heat of formation of PH_3 while Rossini *et al.* (10) list a value of 2.21 Kcal./mole for this quantity. Phosphine has a

Table 20. Physical properties of phosphine

Property	Value
Melting point	-132.5° C.
Boiling point	-87.4° C.
Density	0.146 g/cc at -90°C.
Heat of formation	2.3 Kcal./mole

pyramidal structure with a P-H bond distance of 1.42 A.U. and a bond angle of 93° according to Stevenson (11). Bartell and Hirst's (50) electron diffraction value of ~1.419 A.U. has corroborated this calculation. Phosphine is a much weaker base than ammonia which is indicated by its limited solubility in water and the absence of a series of phosphonium salts comparable in characteristics to the ammonium salts (51). It is a good reducing agent, reacting with many heavy metal salts such as silver nitrate to form the free metal or metallic phosphides.

Diphosphine may be prepared by the neutral hydrolysis of calcium phosphide according to the procedure of Evers and Street (52). These investigators report the material to be quite unstable, decomposing in the liquid state to P_2H and phosphine.

Neuert and Clasen's (12) results for the fragmentation pattern of phosphine concur with those reported here and with those of the American Petroleum Institute (53, p. 1219). The former investigators' appearance potential measurements are in much closer agreement with the values found here than their previously mentioned measurements on other hydrides.

B. Experimental

1. Preparation

Phosphine for this study was prepared by the method of Paddock (49). Twenty-six millimoles of phosphorus trichloride were added to 58 millimoles of lithium aluminum hydride in 50 milliliters of diethyl ether at 0° C. over a period of 15 minutes. The reaction equation is:

$$4\ PCl_3 + 3\ LiAlH_4 = 4\ PH_3 + 3\ LiCl + 3\ AlCl_3. \qquad (46)$$

The gases formed were condensed in two liquid nitrogen-cooled traps. The first trap was then allowed to warm to the temperature of a chloroform slush bath (-63.5° C.), the phosphine distilling into the second trap. The second trap was then isolated, allowed to warm to -63.5° C. and the phosphine collected. Mass spectral analysis showed the gas to be pure phosphine; i.e., diphosphine, if formed in the above reaction, was absent. Since no diphosphine was observed in any of the subsequent fractions collected from

this preparation, another method was used to obtain the dihydride. This preparation consisted of two steps: first, the hydrolysis of phosphorous trichloride, giving hydrochloric acid and phosphorous acid, H_3PO_3, and then heating the hydrolysis products under vacuum, the phosphorous acid disproportionating. The mechanism of the formation of diphosphine from this reaction is obscure. Remy (25) reports that phosphoric acid and phosphine are formed by this disproportionation, but after phosphine had been separated and collected, mass spectral analysis of the gases remaining in the system indicated the existence of diphosphine. The usual inflammability of diphosphine was observed.

2. Mass spectral properties

a. Fragmentation patterns The mass spectrum of phosphine is shown in Figure 19. Since phosphorus is anisotopic the spectrum is simple and easily interpreted. As mentioned earlier, the fragmentation pattern concurs with the work of Neuert and Clasen (12) and with the results compiled by the American Petroleum Institute (53, p. 1219). The conditions in the ion source were consistent with those previously described on page 34. The mass scale was calibrated with the known isotopes of sulfur by observing the S^+ fragment from SO_2. Sulfur dioxide was also used to calibrate the mass scale of diphosphine, using the parent fragment. The corrected fragmentation pattern of phosphine is

Figure 19. The mass spectrum of phosphine

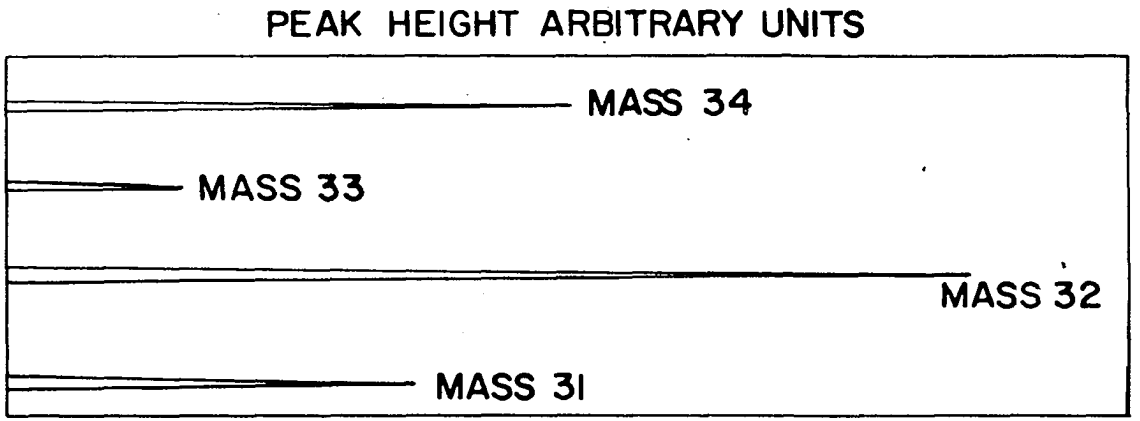
PEAK HEIGHT ARBITRARY UNITS
MASS 34
MASS 33
MASS 32
MASS 31

listed in Table 21.

Diphosphine's mass spectrum is shown in Figure 20 and the fragmentation pattern corrected for pressure and gas flow change in Table 22. No values are listed for the monophosphorus ions in Table 22 because the abundances of these ions were so small the values could not be reproduced. From the fragmentation pattern it seems likely that the P-P bond is the strongest in the molecule. This hypothesis could not be tested further since any appearance potential measurements would be meaningless. The reason for this is the ion intensities were diminutive and numerous processes were occurring in the ion source.

Table 21. Fragmentation pattern of phosphine

Ion	Relative peak height
PH_3^+	68.0
PH_2^+	25.4
PH^+	100.0
P^+	40.2

Figure 20. The mass spectrum of diphosphine

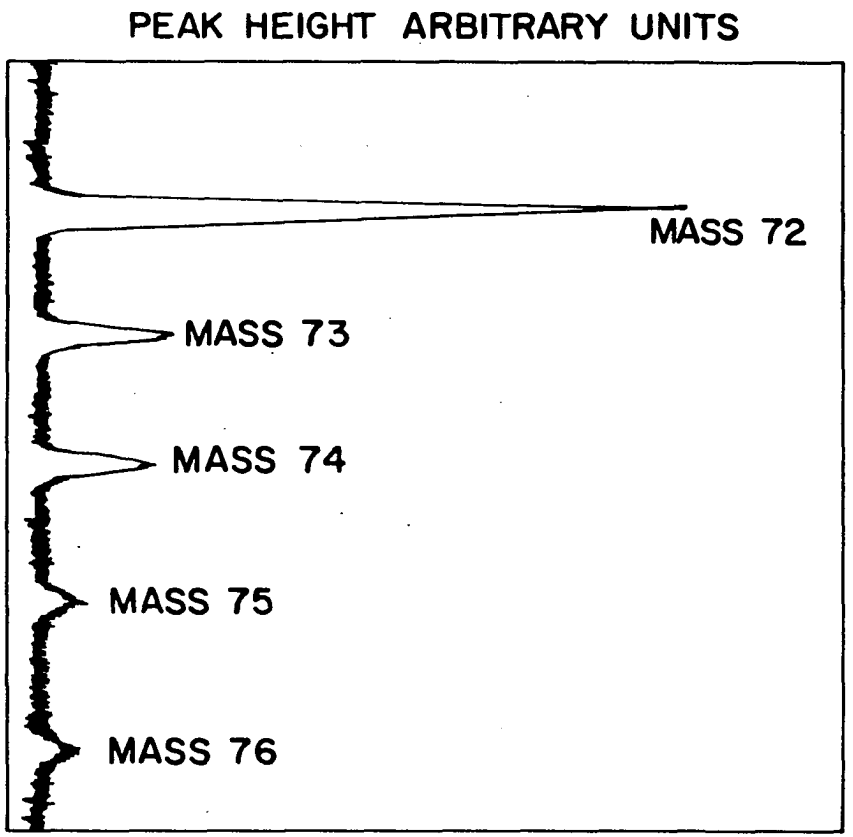
PEAK HEIGHT ARBITRARY UNITS
MASS 72
MASS 73
MASS 74
MASS 75
MASS 76

Table 22. Fragmentation pattern of diphosphine

Ion	Relative peak height
$P_2H_4^+$	6.2
$P_2H_3^+$	11.7
$P_2H_2^+$	32.6
P_2H^+	25.4
P_2^+	100.0

b. Appearance potentials The method of taking the data was the same as used for the previously discussed hydrides (14). The ionization efficiency curves are shown in Figure 21 and appearance potentials and their associated processes in Table 23. Argon was used as an internal standard to calibrate the voltage scale.

When the appearance potential given in Equation 51 is used in Equation 11 along with the heat of formation of P^+ (16) a value of 1.4 $\pm$ 4 Kcal./mole is obtained for the standard heat of formation of phosphine. This concurs with the value of 1.3 Kcal./mole reported by Gunn and Green (9) but is lower than the 2.21 Kcal./mole cited by Rossini et al. (10). The average P-H bond energy can be calculated with

Figure 21. Appearance potential curves of phosphine
Argon is used as an internal standard.

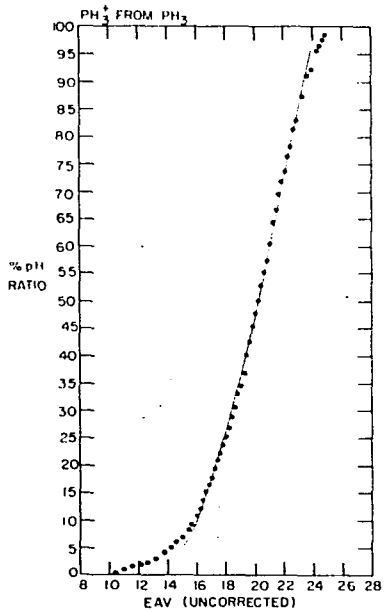
PH_3^+ FROM PH_3
% pH RATIO
EAV (UNCORRECTED)

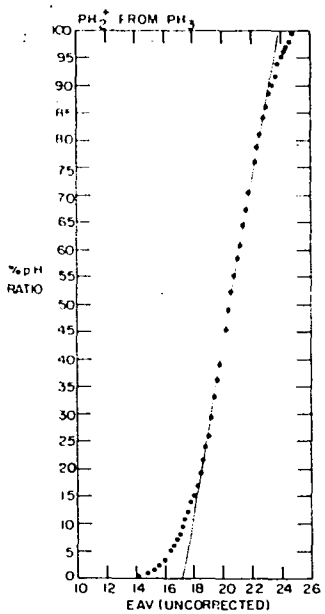
PH_2^+ FROM PH_3
% pH RATIO
EAV (UNCORRECTED)

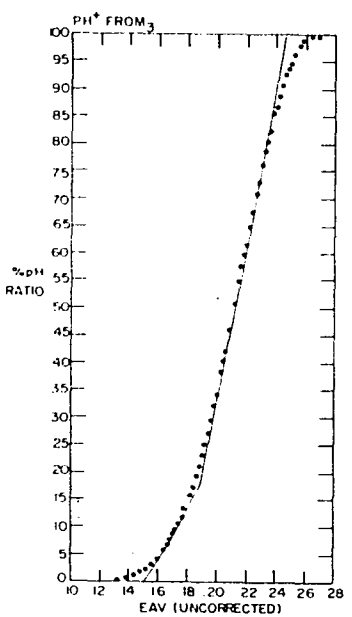
PH^+ FROM PH_3
% pH RATIO
EAV (UNCORRECTED)

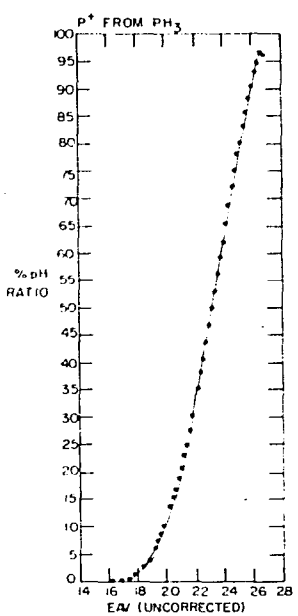
P^+ FROM PH_3
% pH RATIO
EAV (UNCORRECTED)

Table 23. Appearance potentials and processes involved in the formation of the fragment ions from phosphine

Ion	Appearance potential	Process	
PH_3^+	11.5 ± 0.3 e.v.	$PH_3 + e = PH_3^+ + 2e$	(47)
PH_2^+	14.4 ± 0.2	$PH_3 + e = PH_2^+ + H + 2e$	(48)
PH^+	12.4 ± 0.2	$PH_3 + e = PH^+ + H_2 + 2e$	(49)
	16.4 ± 0.3	$PH_3 + e = PH^+ + 2H + 2e$	(50)
P^+	16.5 ± 0.2	$PH_3 + e = P^+ + H_2 + H + 2e$	(51)
	20.8 ± 0.3	$PH_3 + e = P^+ + 3H + 2e$	(52)

Equation 12 by using the same process, Equation 51, and the spectroscopic ionization potential of 11.0 electron volts (18). The 76.8 ± 4 Kcal./mole agrees well with values cited by Gunn and Green, 76.8 Kcal./mole (9); Cottrell, 77 Kcal./mole (19); Huggins, 77 Kcal./mole (40); and with the flash photolysis value of 75 Kcal./mole by Norrish and Oldershaw (54). The P^+ fragment was tested for kinetic energy by the method of Taubert (5) and no such energy was found. It therefore was assumed that the higher mass fragments contained negligible kinetic energy.

The bond energies of the various ion fragments may be

calculated using the processes and equations cited in Table 24. The bond energies are given in Table 25. The large value for the P^+-H bond energy supports the observation that PH^+ is the major ion fragment in the spectrum. The fact that PH^+-H bond energy was found to be the weakest bond substantiates the fact that PH_2^+ is the least abundant of the ion fragments.

c. Cross-sections The relative ionization cross-section of phosphine is 16.8 and that of diphosphine is 31.6 (21).

Table 24. Processes and equations for determining the bond energies of the ion fragments of phosphine

Process	Equation
$PH_3 + e = PH_3^+ + 2e$	$A.P._1 = I.P.(PH_3) = 11.5$ e.v. (53)
$PH_3 + e = PH_2^+ + H + 2e$	$A.P._2 = A.P._1 + D.E.(PH_2^+-H) = 14.4$ (54)
$PH_3 + e = PH^+ + 2H + 2e$	$A.P._3 = A.P._2 + D.E.(PH^+-H) = 16.4$ (55)
$PH_3 + e = P^+ + 3H + 2e$	$A.P._4 = A.P._3 + D.E.(P^+-H) = 20.8$ (56)

Table 25. Dissociation energies of the various ion fragments of phosphine

Ion fragment	Dissociation energy
PH_2^+-H	2.9 e.v.
PH^+-H	2.0
P^+-H	4.4

VII. ARSINE

A. Introduction

Scheele discovered arsine in 1775 when he combined arsenic acid, H_3AsO_4, with metallic zinc (47). Arsine also can be formed by the hydrolysis of active metal arsenide such as Na_3As or Zn_3As_2. Nearly pure arsine may be obtained if sodium arsenide is treated in liquid ammonia with ammonium bromide. In the prepration of Jolly and Drake (31) arsenic III oxide was reduced with an aqueous borohydride solution. Their prepration was very similar to that of Kramer (46). Diarsine, As_2H_4, is formed as a byproduct of Jolly and Drake's reaction (31) but may easily be separated from arsine.

Moist arsine rapidly decomposes to arsenic on exposure to light but the pure dry gas is stable (55). If arsine is ignited it burns with a bluish flame to arsenic trioxide. When the gas is passed through a heated tube, arsine decomposes to the elements leaving a lustrous black metallic mirror just beyond the heated zone. Arsine will reduce a dilute silver nitrate solution to free silver and arsenious acid, H_3AsO_3, but a concentrated solution of silver nitrate will form the molecular addition compound silver arsenide and silver nitrate, $Ag_3As \cdot 3AgNO_3$ (47).

Arsine is a colorless, poisonous gas which, like

ammonia and phosphine, has a pyramidal structure. Stevenson (11) has predicted the H-As-H bond angles to be close to 90° and the A-H bond distance 1.53 A.U. Nielsen's (56) infrared work gives 91°35' for the angle and 1.523 A.U. for the bond distance. Some physical properties of arsine, as cited by Hurd (6), are listed in Table 26. The value for the heat of formation given in this table differs considerably from 15.9 Kcal./mole by Gunn and Green (9) and 18 Kcal./mole by Ariya et al. (57).

There are no detail mass spectral reports of arsine. A private communication[1] from the Lawrence Radiation Laboratory giving the fragmentation pattern of arsine was the only mass spectral information available. Neuert and Clasen (12) claimed that arsine could not be measured in their mass spectrometer due to thermal dissociation.

Table 26. Physical properties of arsine

Property	Value
Melting point	-113.5° C.
Boiling point	-55.0° C.
Heat of formation	-43.49 Kcal./mole

[1]Lawrence Radiation Laboratory, University of California, Berkeley, California. The uncertified mass spectrum of arsine. Private communication (1959).

B. Experimental

1. Preparation

Arsine and diarsine were prepared by the reduction of arsenic trichloride with sodium borohydride. A 25 milliliter solution of 2.5 milliliters of concentrated hydrochloric acid and 0.5 milliliter of arsenic trichloride was added to a 10 per cent solution of aqueous sodium borohydride over a period of 10 minutes. The borohydride solution was stirred magnetically and nitrogen was used as a carrier gas to flush the products from the reaction flask. The gaseous products were swept through a chloroform-slush bath to remove the water. Arsine and diarsine were then condensed in a liquid nitrogen-cooled trap. The nitrogen-cooled trap was isolated, evacuated, and the arsine and diarsine were separated by fractionation through a trap cooled by a chloroform-slush bath. Mass spectral analysis showed the separation to be complete.

2. Mass spectral properties

a. Fragmentation patterns The mass spectrum of arsine is shown in Figure 22 and that of diarsine in Figure 23. The fragmentation patterns, corrected for pressure and gas flow change, are listed in Tables 27 and 28 respectively. The ion source conditions are the same as described on page 34. No monomeric ions are listed in

Figure 22. The mass spectrum of arsine

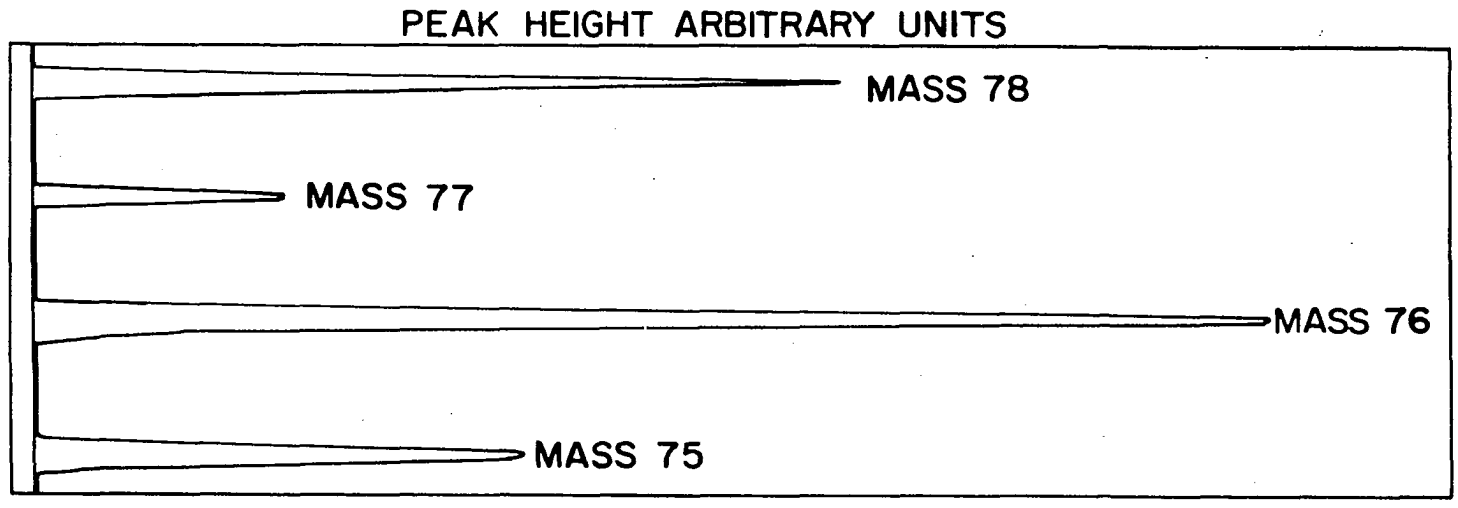
PEAK HEIGHT ARBITRARY UNITS
MASS 78
MASS 77
MASS 76
MASS 75

Figure 23. The mass spectrum of diarsine

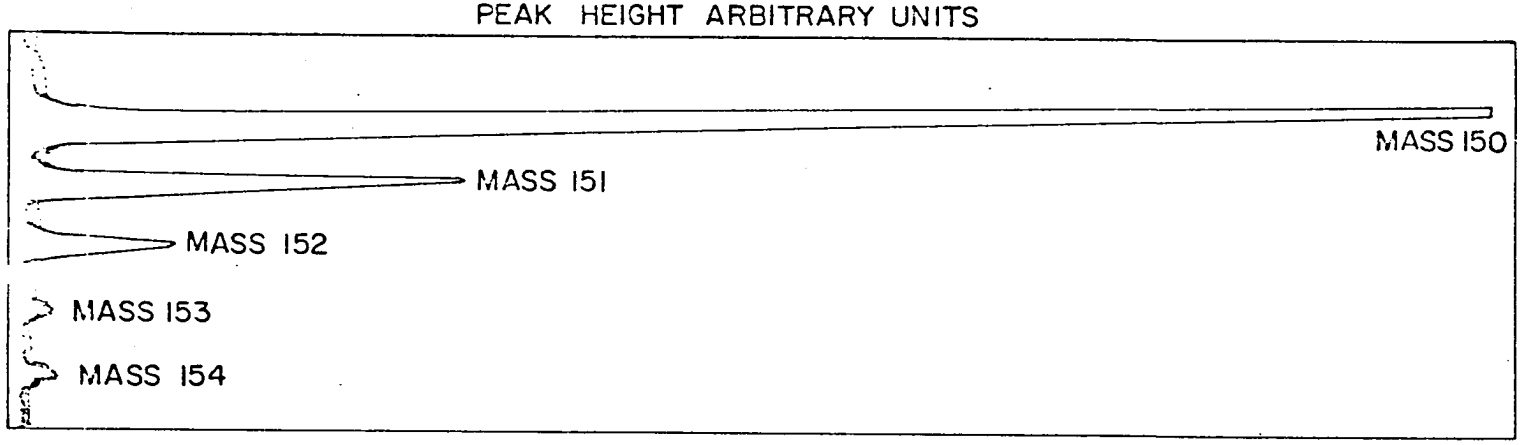
PEAK HEIGHT ARBITRARY UNITS
MASS 150
MASS 151
MASS 152
MASS 153
MASS 154

Table 27. Fragmentation pattern of arsine

Ion	Relative peak height
AsH_3^+	66.5
AsH_2^+	22.3
AsH^+	100.0
As^+	40.4

Table 28. Fragmentation pattern of diarsine

Ion	Relative peak height
$As_2H_4^+$	3.0
$As_2H_3^+$	1.4
$As_2H_2^+$	7.3
As_2H^+	21.7
As_2^+	100.0

Table 28 for the same reasons discussed on page 90.

The mass scale of arsine and diarsine was calibrated by comparison with the known peaks of germane and digermane respectively. From the fragmentation pattern of diarsine the As-As bond appears to be the strongest in the molecule although this cannot be stated with certainty due to the difficulties described in section VI, 2a.

b. Appearance potentials The method of taking the appearance potential data is the same as previously discussed (14) and the ionization efficiency curves are shown in Figure 24. The appearance potentials and their associated processes are listed in Table 29. Argon was used as an internal standard to calibrate the voltage scale. Two additional "breaks" were observed in the As^+ ionization

Table 29. Appearance potentials and processes involved in the formation of the ion fragments from arsine

Ion	Appearance potential	Process	
AsH_3^+	12.1 ± 0.2 e.v.	$AsH_3 + e = AsH_3^+ + 2e$	(57)
AsH_2^+	14.5 ± 0.2	$AsH_3 + e = AsH_2^+ + H + 2e$	(58)
AsH^+	12.4 ± 0.2	$AsH_3 + e = AsH^+ + H_2 + 2e$	(59)
	16.8 ± 0.3	$AsH_3 + e = AsH^+ + 2H + 2e$	(60)
As^+	14.8 ± 0.2	$AsH_3 + e = As^+ + H_2 + H + 2e$	(61)
	19.4 ± 0.2	$AsH_3 + e = As^+ + 3H + 2e$	(62)

Figure 24. Appearance potential curves of arsine
Argon is used as an internal standard.

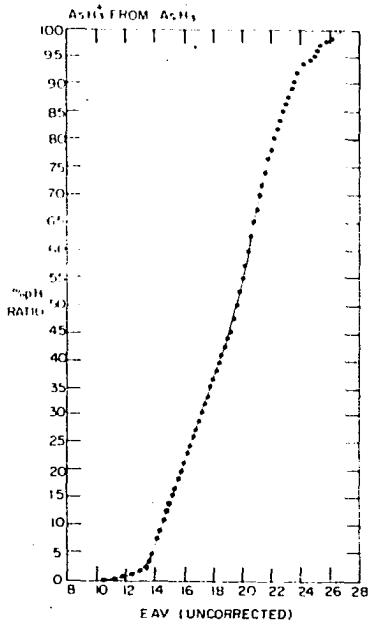
AsH$_2^+$ FROM AsH$_3$
%pH RATIO
E AV (UNCORRECTED)

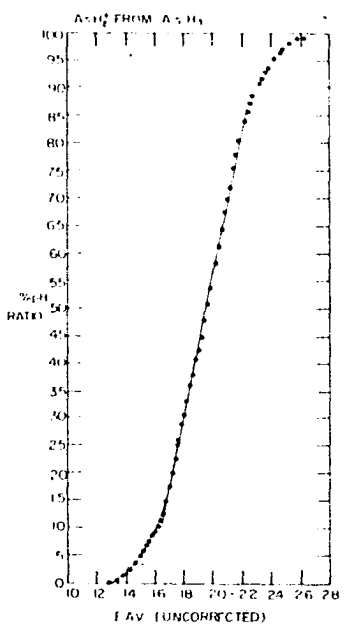
AsH$_2^+$ FROM AsH$_3$
%pH RATIO
E AV (UNCORRECTED)

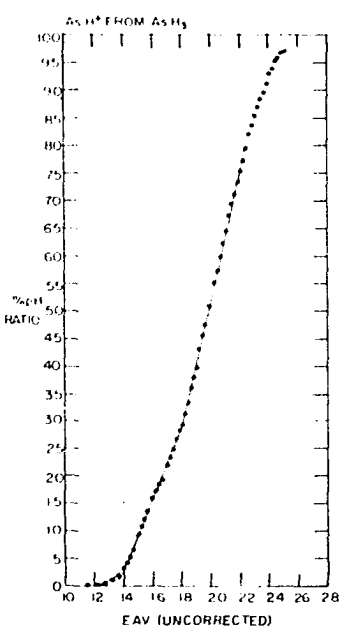
AsH$^+$ FROM AsH$_3$
%pH RATIO
E AV (UNCORRECTED)

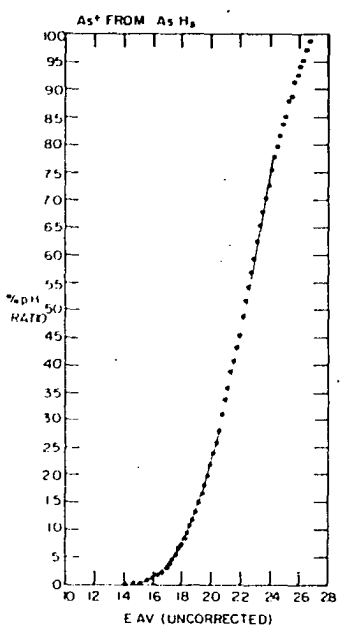
As$^+$ FROM AsH$_3$
%pH RATIO
E AV (UNCORRECTED)

efficiency curve which agreed well with the spectroscopic energy for the excited states $^1D_2$ and $^1S_0$ (58). When the appearance potential given in Equation 61 is combined with the heat of formation of As^+ (16) and used in Equation 12, 15.0 $\pm$ 4 Kcal./mole is found for the standard heat of formation of arsine. This is in good agreement with the values given by Gunn and Green (9) and by Ariya *et al.* (57) but is in poor accord with that of Rossini *et al.* (10) and Hurd (6). The latter two investigators make no mention as to the source of their values so the discrepancy between the above numbers cannot be reconciled.

If the spectroscopic ionization potential (58) and the appearance potential given by Equation 61 are used in Equation 12, the average As-H bond energy is found to be 72.9 $\pm$ 4 Kcal./mole. This concurs with the theoretical value of 71 Kcal./mole by Huggins (40) but differs from Gunn and Green's 66.8 Kcal./mole (9). The As^+ fragment was found to contain no excess kinetic energy when tested by Taubert's (5) method. The absence of this energy was then assumed for the other fragments. The bond energies of the various ion fragments may be found by using the equations and processes in Table 30. The bond energies are shown in Table 31. Since all of the bond dissociation energies are about equal, the fragmentation pattern of arsine is difficult to reconcile with this data.

o. Cross-sections The total relative ionization cross-section of arsine is 21.7 while that of diarsine is 41.4 (21).

Table 30. Processes and equations for determining the bond strength of the ion fragments of arsine

Process	Equation	
$AsH_3 + e = AsH_3^+ + 2e$	$A.P._1 = I.P. = 12.1$ e.v.	(63)
$AsH_3 + e = AsH_2^+ + H + 2e$	$A.P._2 = A.P._1 + D.E.(AsH_2^+-H) = 14.5$	(64)
$AsH_3 + e = AsH^+ + 2H + 2e$	$A.P._3 = A.P._2 + D.E.(AsH^+-H) = 16.8$	(65)
$AsH_3 + e = As^+ + 3H + 2e$	$A.P._4 = A.P._3 + D.E.(As^+-H) = 19.4$	(66)

Table 31. Dissociation energies of the various ion fragments of arsine

Ion fragment	Dissociation energy
AsH_2^+-H	2.4 e.v.
AsH^+-H	2.3
As^+-H	2.6

VIII. STIBINE

A. Introduction

Stibine was discovered independently in 1837 by Thompson and Pfaff (47). These investigators obtained the hydride by reacting a solution of an antimony compound with zinc and dilute sulfuric acid. Hydrolysis of several antimony alloys such as zinc-antimony or magnesium-antimony is a good synthesis for stibine. Stibine may also be prepared by the electrolysis of acid or alkaline solutions with a cathode of metallic antimony giving yields of 15 per cent (59). Traces of hydrocarbons are claimed to catalyze the formation of small amounts of stibine from the reaction of atomic hydrogen on metallic antimony (6). The reduction of potassium antimony tartrate by potassium borohydride has been reported by Gunn et al. (60). Their reaction is quite similar to the one reported by Kramer (46).

Stibine is a colorless gas with a pungent odor and is even more toxic than arsine. It has a pyramidal structure like the rest of the group VB hydrides. Stevenson (11) has predicted a H-Sb-H bond angle of close to 90° and a Sb-H bond distance of 1.73 A.U. These values concur with those of Nielsen (56) who found the bond angle to be $91^{\circ}30'$ and the bond distance 1.711 A.U. Some physical properties of stibine are given in Table 32 (6). Stock and Wrede (61)

Table 32. Physical properties of stibine

Property	Value
Melting point	-88.5° C.
Boiling point	-17.0° C.
Density at boiling point	2.204 g/cc

report 34.27 Kcal./mole for the heat of formation of stibine. This value agrees with that obtained by Gunn and Green (9).

Stibine will reduce a solution of silver nitrate forming silver antimonide Ag_3Sb, but this compound is rapidly decomposed by excess silver nitrate to a mixture of silver, antimony trioxide and antimony (47). Stibine is only slightly soluble in water but extremely soluble in carbon disulfide (6). When a mixture of stibine and hydrogen is directly ignited it burns with a green flame (25). Stibine passing through a heated tube is decomposed into the elements leaving a black metallic mirror on the wall of the tube on both sides of the heated zone. This can be distinguished from the arsenic mirror since it is not affected by treatment with a sodium hypochlorite solution (25). Jolly

and Drake (31) have reported that stibine lies between arsine and stannane in its stability. They also state that if stibine is to be stored longer than two or three days it should be kept frozen with liquid nitrogen. While the instability just described for stibine was affirmed here, stannane prepared in these laboratories was more stable than stibine (37).

B. Experimental

1. Preparation

Stibine was prepared by the addition of a 50 milliliter solution containing 0.5 gram of antimony trichloride and 3 milliliters of concentrated hydrochloric acid to a 10 per cent aqueous sodium borohydride solution over a period of 20 minutes. The reaction vessel was swept with nitrogen throughout the addition and the borohydride solution stirred magnetically. The gases were swept through a trap at -16°C (an aqueous solution of 24 per cent by weight methanol at its melting point) to remove the water vapor and then condensed in a liquid nitrogen-cooled trap. The nitrogen-cooled trap was then isolated and evacuated. The products were condensed and then were fractionated through traps at -22.4° C. (carbon tetrachloride at its melting point) and -16° C. The gases were collected and analyzed on the mass spectrometer. Except for traces of water and carbon

dioxide, the gas was pure stibine. After stibine had been collected, the system was evacuated and then the various traps allowed to warm to room temperature. The gas that was then found in the system was collected and analyzed on the mass spectrometer. The first attempted preparation of stibine was analyzed on the mass spectrometer described by Flesch and Svec (36). This analysis showed the existence of distibine in the second sample collected. Subsequent analyses of the same fraction from several other preparations on the instrument described in this thesis did not reproduce these findings. There was only 1 part of dimer to 300 parts of monomer observed in the first measurement. Since the sensitivity of the present mass spectrometer is lower than that of the first, this may explain the absence of this species. More evidence for the existence of distibine was obtained by the following procedure. After the stibine had been collected, the system was evacuated at a temperature where SbH_3 is a gas and then isolated. The cold traps were removed and the system was allowed to warm to room temperature. A black metallic mirror formed in the system. The mirror could not have been from stibine because the hydride was completely removed by the evacuation. This mirror gave a positive spot test (42) for antimony. Also the rate of decomposition observed was much faster than with the stibine previously collected. One small peak was observed in the

dimer region on the present instrument. It is possible that the peaks of distibine, being very small, were obscured by the zero noise level of the vibrating reed electrometer. More work will be undertaken on distibine later.

2. Mass spectral properties

a. Fragmentation pattern Figure 25 shows the mass spectrum of stibine and the relative ion intensities, corrected for gas flow change, along with the positive ion types are given in Table 33. The fragmentation pattern, calculated from the known isotope abundances (13), is given in Table 34. Stannane was used to calibrate the mass scale. Ion source conditions have not been changed from those previously described on page 34.

The corrected relative ion intensities of distibine and its positive ion fragments are given in Table 35 while the fragmentation pattern, calculated from the isotope abundances given by Bainbridge and Nier (13), is shown in Table 36. This spectrum, as mentioned previously, was obtained on the instrument discussed by Flesch and Svec (35). Since the data could not be reproduced, it must be considered tenuous at present. The mass scale in the distibine region was not calibrated. Like diphosphine and diarsine the metal-metal ion fragment was the largest peak observed, indicating that the Sb-Sb bond is the strongest in the molecule.

Figure 25. The mass spectrum of stibine

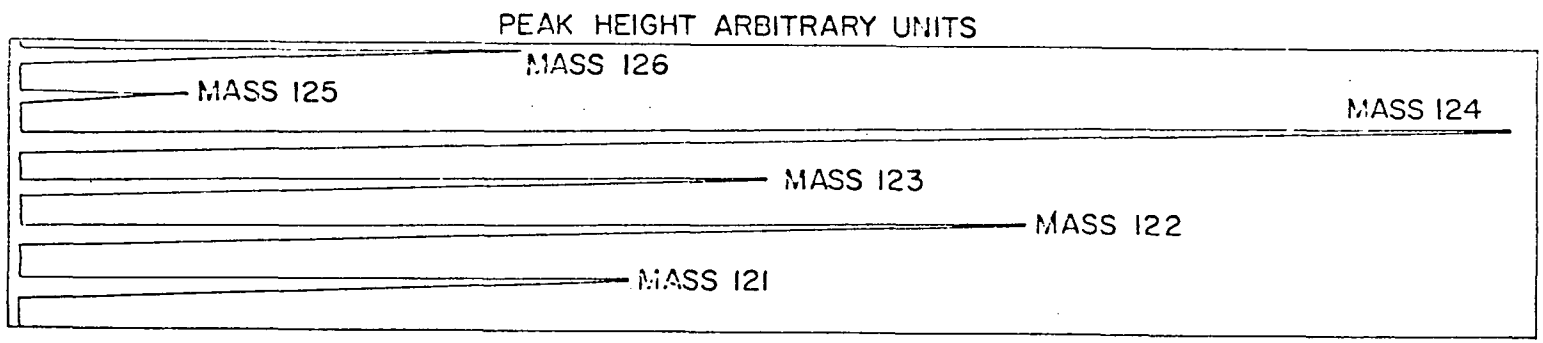
PEAK HEIGHT ARBITRARY UNITS
MASS 126
MASS 125
MASS 124
MASS 123
MASS 122
MASS 121

Table 33. Relative intensities and positive ion types of stibine

Mass	Relative peak height	Positive ions	
126	37.7	$^{123}SbH_3^+$	
125	16.2	$^{123}SbH_2^+$	
124	100.0	$^{123}SbH^+$	$^{121}SbH_3^+$
123	53.9	$^{123}Sb^+$	$^{121}SbH_2^+$
122	67.8		$^{121}SbH^+$
121	43.6		$^{121}Sb^+$

Table 34. Fragmentation pattern of stibine

Antimony isotope	SbH_3^+	SbH_2^+	SbH^+	Sb^+
121	73.8	31.8	100.0	63.7
123	73.9	31.8	100.0	63.8

Table 35. Relative ion intensities and positive ion types of distibine

Mass	Relative peak height	Positive ions		
250	0.5	$^{123}Sb_2H_4^+$		
249	0.7	$^{123}Sb_2H_3^+$		
248	2.4	$^{123}Sb_2H_2^+$	$^{123}Sb^{121}SbH_4^+$	
247	28.2	$^{123}Sb_2H^+$	$^{123}Sb^{121}SbH_3^+$	
246	53.4	$^{123}Sb_2^+$	$^{123}Sb^{121}SbH_2^+$	$^{121}Sb_2H_4^+$
245	56.4		$^{123}Sb^{121}SbH^+$	$^{121}Sb_2H_3^+$
244	100.0		$^{123}Sb^{121}Sb^+$	$^{121}Sb_2H_2^+$
243	32.4			$^{121}Sb_2H^+$
242	52.3			$^{121}Sb_2^+$

Table 36. Fragmentation pattern of distibine

Antimony isotope	$Sb_2H_4^+$	$Sb_2H_3^+$	$Sb_2H_2^+$	Sb_2H^+	Sb_2^+
123 - 123	< 0.1	15.0	41.6	62.5	100.0
123 - 121	< 0.1	14.9	40.9	62.0	100.0
121 - 121	< 0.1	14.9	41.0	62.0	100.0

b. Appearance potentials The method of obtaining the data for the ionization efficiency curves has not been changed from that delineated previously (14). The curves are shown in Figure 26. Like the As^+ fragment, an additional "break" was observed in the ionization efficiency curve of Sb^+ which agreed with the spectroscopic energy (58) for the $^1S_0$ state. The appearance potentials and their associated processes are listed in Table 37. Argon was used as an internal standard to calibrate the voltage scale.

Table 37. Appearance potentials and processes involved in the formation of the fragment ions from stibine

Ion	Appearance potential	Process	
SbH_3^+	9.9 ± 0.3 e.v.	$SbH_3 + e = SbH_3^+ + 2e$	(67)
SbH_2^+	11.8 ± 0.3	$SbH_3 + e = SbH_2^+ + H + 2e$	(68)
SbH^+	9.9 ± 0.2	$SbH_3 + e = SbH^+ + H_2 + 2e$	(69)
	14.2 ± 0.3	$SbH_3 + e = SbH^+ + 2H + 2e$	(70)
Sb^+	12.1 ± 0.2	$SbH_3 + e = Sb^+ + H_2 + H + 2e$	(71)
	16.7 ± 0.3	$SbH_3 + e = Sb^+ + 3H + 2e$	(72)

Figure 26. Appearance potential curves of stibine
Argon is used as an internal standard.

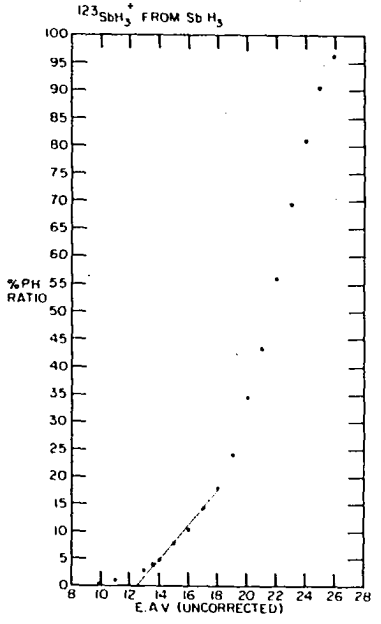
$^{123}SbH_3^+$ FROM SbH_3
%PH RATIO
E.A.V (UNCORRECTED)

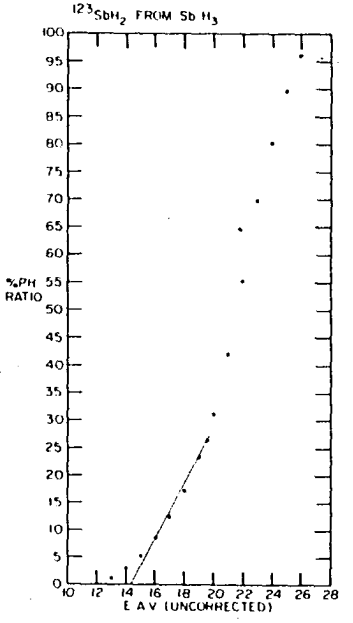
$^{123}SbH_2$ FROM SbH_3
%PH RATIO
E.A.V (UNCORRECTED)

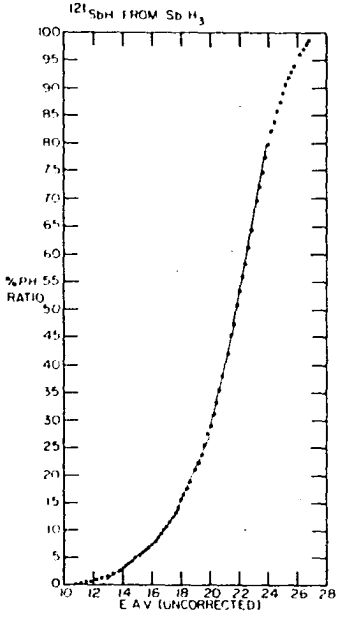
^{121}SbH FROM SbH_3
%PH RATIO
E.A.V (UNCORRECTED)

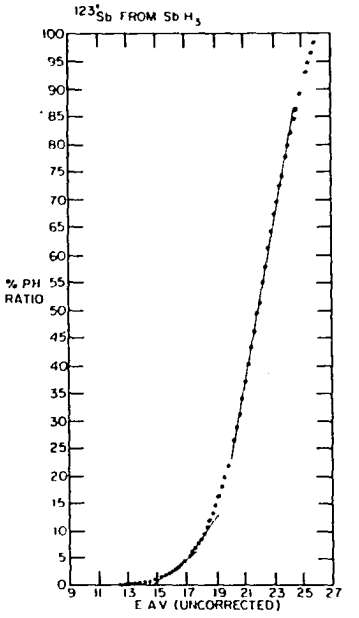
^{123}Sb FROM SbH_3
%PH RATIO
E.A.V (UNCORRECTED)

If the appearance potential given in Equation 71 is combined with the heat of formation of Sb^+ (16) and used in Equation 11, the standard heat of formation of stibine is found to be 34.6 ± 4 Kcal./mole. This concurs with the value of 34.7 Kcal./mole by Gunn and Green (9) and with the value cited by Stock and Wrede (61). Using the spectroscopic ionization potential given by Moore (58), the average Sb-H bond energy is found to be 61.1 ± 4 Kcal./mole which essentially agrees with that of Gunn and Green (9). The Sb^+ fragment was found to contain no excess kinetic energy. The heavier ions were then assumed to contain no excess energy.

Using the processes and equations listed in Table 38, the bond energies of the various ion fragments were calculated. These values are given in Table 39.

Table 38. Processes and equations for determining the bond strengths of the ion fragments of stibine

Process	Equation	
$SbH_3 + e = SbH_3^+ + 2e$	$A.P._1 = I.P. = 9.9$ e.v.	(73)
$SbH_3 + e = SbH_2^+ + H + 2e$	$A.P._2 = A.P._1 + D.E.(SbH_2^+-H) = 11.8$	(74)
$SbH_3 + e = SbH^+ + 2H + 2e$	$A.P._3 = A.P._2 + D.E.(SbH^+-H) = 14.2$	(75)
$SbH_3 + e = Sb^+ + 3H + 2e$	$A.P._4 = A.P._3 + D.E.(Sb^+-H) = 16.7$	(76)

Table 39. Dissociation energies of the various ion fragments of stibine

Ion fragment	Dissociation energy
SbH_2^+-H	1.9 e.v.
SbH^+-H	2.4
Sb^+-H	2.5

The fact that the Sb^+-H bond is the strongest supports the observation that the SbH^+ fragment is the most abundant in the spectrum. However, since the three bond energies are so nearly equal, the above interpretation must be considered tenuous.

c. Cross-sections The cross-section of stibine is 29.1 and that of distibine is 56.2 (21).

IX. BISMUTHINE

A. Introduction

Bismuthine was first prepared by Paneth (62) who hydrolyzed an alloy of magnesium and the radioactive isotope of bismuth, thorium C. By treating a finely divided mixture of bismuth and magnesium, Paneth and Winternitz (63) found that bismuthine could be prepared from normal bismuth. The sodium alloy of bismuth, Na_3Bi, gives no bismuthine upon hydrolysis (64). Kramer (46) reported that the sodium borohydride reduction of bismuth nitrate yielded insufficient amounts of bismuthine. The hydride that did form was claimed to have been fused with the glass. Recently, Amberger (65) prepared bismuthine by the reduction of bismuth trichloride with lithium aluminum hydride at -110° C. He claimed that bismuthine decomposed on the glass surface at room temperature. Bismuthine is said to be more toxic than either arsine or stibine (6).

B. Experimental

Bismuthine was prepared by reducing a 0.6 normal hydrochloric acid solution containing 0.5 gram of bismuth trichloride with a 10 per cent aqueous sodium borohydride solution. The gases formed were condensed in a liquid nitrogen-cooled trap. The cold trap was isolated, evacuated and

allowed to warm to room temperature. The gas was collected and analyzed in the mass spectrometer. Results of this analysis were negative, but a black metallic mirror was observed to form in the cold trap when it was warmed to room temperature. This was shown to be a mirror bismuth by a spot test (42). It was assumed then, as Amberger later reported, that the decomposition depended on the glass surface. The vacuum line was subsequently lined with a paraffin coating and the preparation repeated. This time the mirror formed on top of the wax and again no bismuthine was observed in the mass spectrometer. The formation of a bismuth mirror on the wax surface indicated that bismuthine does not need a glass surface in order to decompose at room temperature.

X. SUMMARY

The hydrides of groups IVB and VB have been prepared by a reduction of various compounds, in most cases chlorides, with either sodium borohydride or lithium aluminum hydride. These hydrides except plumbane, bismuthine, methane and ammonia have been analyzed in the mass spectrometer and their fragmentation patterns and appearance potentials reported. The fragment ions have been checked for kinetic energy and this energy was found to be negligible. Several of the dihydrides have been observed and fragmentary evidence for the existence of distibine has been cited. The hydrides of lead and bismuth did not lend themselves to mass spectral analysis because of their instability.

The bond energies and heats of formation for the hydrides have been calculated and are summarized along with the mass spectral data in the appendices.

The agreement of mass spectra values for the bond energies and heats of formation with other methods of determining these quantities indicates that mass spectral data are reliable sources for these energies.

XI. BIBLIOGRAPHY

1. Svec, H. J. Mass spectrometry. Unpublished Ph.D. Thesis. Ames, Iowa, Library, Iowa State University of Science and Technology. (1950).

2. Barnard, G. P. Modern mass spectrometry. London, England, The Institute of Physics. (1953).

3. Duckworth, Henry E. Mass spectroscopy. Cambridge, England, Cambridge University Press. (1958).

4. Beynon, J. H. Mass spectrometry and its applications to organic chemistry. Amsterdam, The Netherlands, Elsevier Publishing Company. (1960).

5. Taubert, R. Kinetic energy of fragment ions. In Waldron, J. D., ed. Advances in mass spectrometry. pp. 489-503. London, England, Pergamon Press. (1959).

6. Hurd, D. T. An introduction to the chemistry of the hydrides. New York, N. Y., John Wiley and Sons Inc. (1952).

7. Johnson, W. C. and Hogness, T. R. J. Am. Chem. Soc. 56 1252 (1934).

8. Finholt, A. E., Bond, A. C., Wilzback, K. E. and Schlesinger, H. L. J. Am. Chem. Soc. 69 2692 (1947).

9. Gunn, S. R. and Green, L. G. J. Phys. Chem. 65 779 (1961).

10. Rossini, F. D., Wagman, D. D., Evans, W. H., Levine, S. and Jaffe, I. Selected values of chemical thermodynamic properties. National Bureau of Standards Circular 500. (1952).

11. Stevenson, D. P. J. Chem. Phys. 8 285 (1940).

12. Neuert, H. and Clasen, H. Z. Naturforschg. 71A 410 (1952).

13. Bainbridge, K. T. and Nier, A. O. Relative isotopic abundances of the elements. Nat. Research Council Nuclear Science Series. Preliminary Report No. 9. (1950).

14. Saalfeld, F. E. The mass spectrum of stannane. Unpublished M. S. Thesis. Ames, Iowa, Library, Iowa State University of Science and Technology. (1959).

15. Vought, R. H. Phys. Rev. 71 93 (1947).

16. Latimer, W. M. Oxidation potentials. 2nd ed. Englewood Cliffs, New Jersey, Prentice Hall, Inc. (1952).

17. Field, F. H. and Franklin, J. L. Electron impact phenomena and the properties of gaseous ions. New York, N. Y., Academic Press, Inc. (1957).

18. Moore, C. E. Atomic energy levels. Vol. 1. National Bureau of Standards. Circular 467. (1949).

19. Cottrell, T. L. The strength of chemical bonds. 2nd ed. London, England, Butterworth Scientific Publications. (1958).

20. Washburn, R. M. and Berry, C. E. Phys. Rev. 70 559 (1946).

21. Otvos, J. W. and Stevenson, D. P. J. Am. Chem 78 546 (1956).

22. Bethe, H. Ann. Physik. 5 352 (1930).

23. Pauling, L. and Wilson, E. B. Introduction to quantum mechanics. New York, N. Y., McGraw-Hill Book Co. (1935).

24. Eyring, H., Walter, J. and Kimball, G. E. Quantum chemistry. New York, N. Y., John Wiley and Sons, Inc. (1944).

25. Remy, H. Treatise on inorganic chemistry. Vol. 1. Amsterdam, The Netherlands, Elsevier Publishing Co. (1956).

26. Dennis, L. M., Corey, R. B. and Moore, R. W. J. Am. Chem. Soc. 46 657 (1924).

27. Sujishi, S. and Keith, J. N. J. Am. Chem. Soc. 80 4138 (1958).

28. Macklen, E. D. J. Chem. Soc. 1989 (1959).

29. Piper, T. S. and Wilson, M. K. J. Inorg. and Nuclear Chem. 4 22 (1957).

30. Jolly, W. L. J. Am. Chem. Soc. 83 335 (1961).

31. _____ and Drake, J. E. U.S. Atomic Energy Commission Report 9615 California Univ., Los Angeles (1961).

32. Steward, W. B. and Nielson, H. H. Phys. Rev. 48 861 (1935).

33. Mévergnies, M. N. de and Delfosse, J. M. Ann. soc. sci. Bruxelles. Ser. 1, 64 188 (1950). (Original not available; abstracted in Chem. Abstr. 45 10064d (1951).)

34. Sanderson, R. T. Vacuum manipulation of volatile compounds. New York, N. Y., John Wiley and Sons, Inc. (1948).

35. Flesch, G. D. and Svec, H. J. J. Am. Chem. Soc. 80 3189 (1950).

36. _____ and _____. J. Am. Chem. Soc. 81 1787 (1959).

37. Saalfeld, F. E. and Svec, H. J. J. Inorg. and Nuclear Chem. 18 98 (1961).

38. Moore, C. E. Atomic energy levels. Vol. 2. National Bureau of Standards. Circular 467. (1952).

39. May, L. and Dillard, C. R. J. Chem. Phys. 34 694 (1961).

40. Huggins, M. L. J. Am. Chem. Soc. 75 4123 (1953).

41. Jolly, W. L. Angew. Chem. 72 268 (1960).

42. Feigl, F. Qualitative analysis by spot tests. 2nd ed. New York, N. Y., Nordemann Publishing Co. (1939).

43. Kleinberg, J., Argersinger, W. J. and Griswold, E. Inorganic chemistry. Boston, Mass., D. C. Heath and Co. (1960).

44. Paneth, F. and Nörring, O. Chem. Ber. 53 1693 (1920).

45. Paneth, F. Radio-elements as indicators and other selected topics in inorganic chemistry. New York, N. Y., McGraw-Hill Book Co. (1928).

46. Kramer, M. E. Reactions with aqueous sodium borohydride. Unpublished Ph. D. Thesis. St. Louis, Mo., Library, Saint Louis University. (1954).

47. Partington, J. R. General and inorganic chemistry. London, England, Macmillan and Co., Limited. (1951).

48. Addison, W. E. and Plummer, J. Chem. and Ind. (London) 935 (1961).

49. Paddock, N. L. Nature 167 1070 (1951).

50. Bartell, L. S. and Hirst, R. C. J. Chem. Phys. 31 449 (1959).

51. Moeller, T. Inorganic chemistry. New York, N. Y., John Wiley and Sons, Inc. (1952).

52. Evers, E. C. and Street, E. H., Jr. J. Am. Chem. Soc. 78 5726 (1956).

53. Zwolenski, B. J., Danti, A., Kerr, J. T. and Berry, W. T. Mass spectral data. Pittsburgh, Pa., American Petroleum Institute. (1960).

54. Norrish, R. G. W. and Oldershaw, G. A. Proc. Roy. Soc. (London) 2621 1308 (1961).

55. Robertson, R., Fox, J. J. and Hiscocks, E. S. Proc. Roy. Soc. (London) 120 149 (1928).

56. Nielsen, H. H. Chem. Phys. 20 759 (1952).

57. Ariya, S. M., Morozova, M. P. and Khuan, T. T. J. Gen. Chem. U.S.S.R. 26 2023 (1956).

58. Moore, C. E. Atomic energy levels. Vol. 3. National bureau of Standards. Circular 467. (1958).

59. Sand, H. J. S., Weeks, E. J. and Worrell, S. W. J. Chem. Soc. 123 456 (1923).

60. Gunn, S. R., Jolly, W. L. and Green, L. G. J. Phys. Chem. 64 1334 (1960).

61. Stock, A. and Wrede, F. Chem. Ber. 41 540 (1908).

62. Paneth, F. Chem. Ber. 51 1704 (1918).

63. _____ and Winternitz, E. Chem. Ber. 51 1728 (1918).

64. _____, Johannsen, A. and Matthias, M. Chem. Ber. 55 769 (1922).

65. Amberger, E. Chem. Ber. 94 1447 (1961).

XII. ACKNOWLEDGEMENTS

The author gratefully acknowledges the guidance afforded him by Professor Harry J. Svec without whose help and friendly understanding this study could never have been completed. A sincere expression of thanks is extended to Mr. Gerald D. Flesch, whose more than generous help in "trouble shooting" the electronic circuits of the mass spectrometer will be remembered always. Various enlightening discussions with Messrs. Harold A. Belsheim and Arthur R. Anderson, as well as with the other members of Professor Svec's group, were greatly appreciated.

Many people aided in the construction of the mass spectrometer built for this study, and the author takes pleasure in acknowledging the following: Mr. Dale Hilker of the electronics shop who built the magnet current control and power supply; Messrs. E. Russell Clark, Harvey Meyer, Lael Smith and Clarence Haugsted who made many of the mechanical parts of the instrument; Messrs. Evert McKenna and Wayne Jones who assembled the glass portions of the spectrometer.

Finally, the sacrifices made by the author's wife, Elizabeth, to make these years of graduate study as pleasant as possible are gratefully acknowledged.

XIII. APPENDICES

A. Appendix A: Comparison of the Fragmentation Patterns and Bond Energies of the Group IVB Hydrides

The fragmentation pattern of methane is taken from the computation of the American Petroleum Institute (53, p. 1). When the fragmentation patterns of the hydrides of group IVB are revised so that their relative ionization cross-sections are equal to that of methane, (21), the values shown in Table 40 are obtained.

The fact that the XH_4^+ fragment is largest for CH_4^+ and progressively becomes smaller to SnH_4^+ is corroborated by the fact that the stability decreases in this order. That the Sn^+ fragment is the largest of the X^+ fragments indicates that the Sn-H bond energy is the weakest in the hydrides as is expected.

Table 40. Fragmentation patterns of group IVB hydrides on the common ionization cross-section of 8.16 for methane

	C	Si	Ge	Sn
XH_4^+	100.0	0.44	0.18	0.03
XH_3^+	85.7	34.6	34.1	27.4
XH_2^+	16.1	44.3	36.4	14.7
XH^+	8.1	9.0	10.3	5.9
X^+	2.8	9.2	17.3	19.4

There seems to be a "cross over" point in the XH^+ and XH_2^+ fragments. Going horizontally from left to right in Table 40 the values continuously decrease for the XH_4^+ and XH_3^+. This trend is continued in XH_2^+ fragments except for an anomaly at carbon. However, for the XH^+ fragments the trend is reversed, the values increase from left to right with an anomaly at tin. The stability of the ion fragments is summarized in Table 41.

It should be noted that the first row of Table 41 concurs with the heat of formation data on these molecules while the stability sequence indicated by the X^+ fragments agrees with those predicted by the ionization potentials.

Table 41. Stability of the ion fragments of group IVB

Fragment	Decreasing stability →			
XH_4^+	C	Si	Ge	Sn
XH_3^+	C	Si	Ge	Sn
XH_2^+	Si	Ge	C	Sn
XH^+	Ge	Si	C	Sn
X^+	Sn	Ge	Si	C

The ion bond energies of the ion fragments of group IVB hydrides are summarized in Table 42. The bond energies for methane, calculated in the same manner as those for the other hydrides of this group, were based on the preferred appearance potentials cited by Field and Franklin (17).

The first two rows in Table 42 show a smooth trend of decreasing bond energy with increasing atomic number. The last row shows no trend but the third row, except for C or Si, is similar to the first two rows.

Table 42. Bond dissociation energies of the ion fragments of the group IVB hydrides

Bond	C	Si	Ge	Sn
XH_3^+-H	1.5 e.v.	0.4 e.v.	0.3 e.v.	0.2 e.v.
XH_2^+-H	5.7	4.7	4.6	4.5
XH^+-H	2.9	3.9	1.4	0.9
X^+-H	3.8	0.4	1.5	2.2

B. Appendix B: Heats of Formation and Average M-H Bond Energies of the Group IVB Hydrides

Table 43. Heat of formation of the group IVB hydrides

	Gunn and Green (9) (calorimetric)	Rossini et al. (10) (tabulation)	This work (mass spectrometric)
	Kcal./mole	Kcal./mole	Kcal./mole
CH_4	-17.9	-17.9	-
SiH_4	+ 7.3	-14.8	8.5
GeH_4	+21.6	-	21.6
SnH_4	+38.9	-	23.0

Table 44. Average M-H bond energy for the group IVB hydrides

	Gunn and Green (9) (calorimetric)	Huggins (40) (theoretical)	Cottrell (19) (tabulation)	This work (mass spectrometric)
	Kcal./mole	Kcal./mole	Kcal./mole	Kcal./mole
C-H	99.3	-	98.7	-
Si-H	76.5	79.0	76.0	72.2
Ge-H	69.0	74.0	-	68.3
Sn-H	60.4	71.0	74.0	70.3

C. Appendix C: Comparison of the Fragmentation Patterns and Bond Energies of the Group VB Hydrides

The fragmentation patterns of ammonia and hydrazine are taken from the data supplied by the American Petroleum Institute (53, p. 90 and p. 1110). When the fragmentation patterns of the group VB hydrides are altered in such a manner that their ionization cross-sections are the same as ammonia, 6.84 (21), the numbers shown in Table 45 are calculated.

Table 45. Fragmentation patterns of group VB hydrides based on the cross-section of 6.84 for ammonia

	N	P	As	Sb
XH_3^+	100.0	27.7	20.9	17.4
XH_2^+	80.0	10.3	7.0	7.5
XH^+	7.5	40.7	31.5	23.5
X^+	2.2	11.4	12.7	15.0

Table 46. Fragmentation patterns of group VB dihydrides based on the cross-section of 11.68 for hydrazine

	N	P	As	Sb
$X_2H_4^+$	100.0	2.3	0.85	0.21
$X_2H_3^+$	47.3	4.3	0.4	3.1
$X_2H_2^+$	31.3	12.1	2.1	8.5
X_2H^+	40.1	9.4	6.0	12.9
X_2^+	21.4	37.0	28.2	20.7

In Table 45 the same trends are observed as in group IVB. The number of parent ions, XH_3^+, decreased with increasing atomic number concurring with the stability of the molecules. The increase of the X^+ fragment supports the fact that the X-H bond energy decreases with atomic number. The XH^+ ion fragment is the cross-over point, fragments above XH^+ decreasing with atomic number, fragments below increasing. An anomaly is observed with SbH^+. This might be explained by the fact that AsH^+ is low. The fourth period elements are well known for their anomalous behavior exemplified by the fact that both PCl_5 and $SbCl_5$ exist while $AsCl_5$ does not. The anomaly is illustrated further by the

fact that the electronegativity of As is much greater, on the Rochow scale, than P and Sb and that both P and Sb will reduce $AsCl_5$ to As.

Due to insufficient data, no interpretation can be made for the observations in Table 46 other than the trend of the parent fragments $X_2H_4^+$ which agree with the stability of these molecules.

The stability of the ion fragments of the monomeric hydrides of group VB are given in Table 47.

Table 47. Stability of the ion fragments of group VB

Fragment	Decreasing stability →			
XH_3^+	N	P	As	Sb
XH_2^+	N	P	Sb	As
XH^+	P	As	Sb	N
X^+	Sb	As	P	N

The first row of Table 47 correlates with the heat of formation data on these molecules while the last row concurs with the ionization potential data.

Table 48 summarizes the bond energies of the ion fragments. The energies of ammonia were calculated from the

Table 48. Bond energies of the ion fragments of group VB hydrides

Bond	N	P	As	Sb
XH_2^+-H	5.3 e.v.	2.9 e.v.	2.4 e.v.	1.9 e.v.
XH^+-H	8.0	2.0	2.3	2.4
X^+-H	1.2	4.4	2.6	2.5

data given by Field and Franklin (17).

Except for the decrease in energy with increasing atomic number of the XH_2^+-H bond no trends are apparent in Table 48.

D. Appendix D: Heats of Formation and Average M-H Bond Energies of the Group VB Hydrides

Table 49. Heat of formation of group VB hydrides

	Gunn and Green (9) (calori-metric)	Rossini et al. (10) (tabulation)	This work (mass spectro-metric)
	Kcal./mole	Kcal./mole	Kcal./mole
NH_3	-11.0	-11.0	-
PH_3	1.3	2.21	1.4
AsH_3	15.9	41.0	15.0
SbH_3	34.7	-	34.6

Table 50. Average M-H bond energies of the group VB hydrides

	Gunn and Green (9) (calori-metric)	Huggins (40) (theoret-ical)	Cottrell (19) (tabula-tion)	This work (mass spectro-metric)
	Kcal./mole	Kcal./mole	Kcal./mole	Kcal./mole
N-H	93.4	85	85	-
P-H	76.8	77	77	76.8
As-H	66.8	71	66	72.9
Sb-H	60.9	70	-	61.1